

ANALYSIS OF FIBER REINFORCED COMPOSITE VESSEL UNDER  
HYGROTHERMAL LOADING

A THESIS SUBMITTED TO  
THE GRADUATE SCHOOL OF NATURAL AND APPLIED SCIENCES  
OF  
THE MIDDLE EAST TECHNICAL UNIVERSITY

BY

SÜMEYRA SAYMAN

IN PARTIAL FULLFILLMENT OF THE REQUIREMENTS FOR THE DEGREE  
OF  
MASTER OF SCIENCES  
IN  
THE DEPARTMENT OF MECHANICAL ENGINEERING

DECEMBER 2003

Approval of the Graduate School of Natural and Applied Sciences

---

Prof. Dr. Canan Özgen

Director

I certify that this thesis satisfies all the requirements as a thesis for the degree of Master of Science.

---

Prof. Dr. Kemal İder

Head of the Department

This is to certify that we have read this thesis and that in our opinion it is fully adequate, in scope and quality, as a thesis for the degree of Master of Science.

---

Prof. Dr. Levend Parnas

Supervisor

Examining Committee Members

Prof. Dr. Levend Parnas

Prof. Dr. Süha Oral

Prof. Dr. Bülent Doyum

Prof. Dr. Yavuz Yaman

Asst. Prof. Dr. Serkan Dağ

## **ABSTRACT**

### **ANALYSIS OF FIBER REINFORCED COMPOSITE VESSEL UNDER HYGROTHERMAL LOADING**

Sayman, Sümeyra

M.S., Department of Mechanical Engineering

Supervisor: Prof. Dr. Levend Parnas

December 2003, 74 Pages

The aim of this study is to develop an explicit analytical formulation based on the anisotropic elasticity theory that determines the behavior of fiber reinforced composite vessel under hygrothermal loading. The loading is studied for three cases separately, which are plane strain case, free ends and pressure vessel cases. For free-end and pressure vessel cases, the vessel is free to expand, on the other hand for plane strain case, the vessel is prevented to expand. Throughout the study, constant, linear and parabolic temperature distributions are investigated and for each distribution, separate equations are developed. Then, a suitable failure theory is applied to investigate the behavior of fiber reinforced composite vessels under the thermal and moisture effects.

Throughout the study, two computer programs are developed which makes possible to investigate the behavior of both symmetrically and antisymmetrically oriented layers. The first program is developed for plane strain case, where the second one is for pressure vessel and free-end cases.

Finally, several thermal loading conditions have been carried out by changing the moisture concentration and temperature distributions and the results are tabulated for comparison purposes.

Keywords: Fiber reinforced vessel, composite material, pressure vessel, composite cylinders, orthotropic, thermal loading, hygrothermal loading, temperature, moisture

## ÖZ

### HİGROTERMAL YÜKLEME ALTINDAKİ ELYAF TAKVİYELİ KOMPOZİT KAPLARIN ANALİZİ

Sayman, Sümeyra

Yüksek Lisans, Makina Mühendisliği Bölümü

Tez Yöneticisi: Prof. Dr. Levend Parnas

Aralık 2003, 74 Sayfa

Bu çalışmanın amacı, anizotropik elastisite teorisine dayalı olarak higrotermal yükleme altındaki elyaf takviyeli kompozit kapların açık analitik formülasyonunu geliştirmektir. Yükleme üç durum için ayrı çalışılmıştır, bunlar düzlem şekil değiştirme durumu, uçların açık olduğu ve basınçlı kap durumlarıdır. İki ucun açık olduğu ve basınçlı kap durumlarında, kap genişlemeye serbesttir, öbür taraftan düzlem şekil değiştirme durumu için, kabın genişlemesi engellenmiştir. Çalışma boyunca sabit, lineer ve parabolik sıcaklık değişimleri incelenmiş ve her bir değişim için, farklı denklemler geliştirilmiştir. Ardından, termal ve nem etkileri altındaki elyaf takviyeli kompozit kabın davranışını incelemek için uygun bir kırılma teorisi uygulanmıştır.

Bu çalışma boyunca, hem simetrik hem de antisimetrik yönlendirilmiş katların davranışını incelemeyi mümkün kılan iki bilgisayar programı geliştirilmiştir. İlk program düzlem şekil değiştirme durumu için çalışırken, ikinci program iki ucun açık olduğu ve basınçlı kap durumları için çalışmaktadır.

Son olarak, nem katsayısını ve sıcaklık dağılımını değiştirmek suretiyle çeşitli termal yükleme durumları çalışılmış ve sonuçlar mukayese amacıyla tablo olarak sunulmuştur.

Anahtar kelimeler: Elyaf takviyeli kap, kompozit malzeme, basınçlı kap, kompozit silindirler, ortotropik, termal yükleme, higrotermal yükleme, sıcaklık, nem

*To my family*

## **ACKNOWLEDGEMENTS**

First of all, I would like to express my deepest appreciation to my thesis supervisor Prof. Dr. Levend Parnas for his support and guidance throughout this study.

I would also like to express my special thanks to my father Prof. Dr. Onur Sayman who supported me throughout this research.

Special thanks to my company Botas Baku-Tbilisi-Ceyhan Pipeline Project Directorate, and especially to my manager Fügen Kalkanlı for her permission to complete my study within these years.

I also wish to thank my dear friends for their help through the study and listening to my complaints.

And I offer my sincere thanks to my family for their support and courage to finish this thesis with their deepest love.

## TABLE OF CONTENTS

ABSTRACT.....	iii
ÖZ.....	v
ACKNOWLEDGEMENTS.....	viii
LIST OF FIGURES.....	x
LIST OF TABLES.....	xiii
LIST OF SYMBOLS.....	xv
INTRODUCTION.....	1
1.1. Fiber Reinforced Composite Materials.....	1
1.1.1. Fibrous Composite Materials.....	2
1.1.2. Mechanical Behavior of Composite Materials.....	2
1.2. Manufacturing of Fiber-Reinforced Composite Materials.....	4
1.3. Filament Winding.....	5
1.4. Analysis of Hygrothermal Behavior of Composite Materials.....	5
THEORETICAL ANALYSIS.....	10
2.1. Introduction.....	10
2.2. Constitutive Relationships for an Orthotropic Lamina.....	10
2.3. General Relations.....	15
2.3.1 Non-Homogenous Solution.....	20
2.3.2. Constant Temperature Distribution ( $T = T_0$ ).....	21
2.3.3.Linear Temperature Distribution ( $T = \lambda(b - r)$ ).....	22
2.3.4. Parabolic Temperature Distribution ( $T = \lambda(b^2 - r^2)$ ).....	24
2.4. Example: T is constant in a plane strain problem.....	25
2.5. Free-End and Pressure Vessel.....	28
2.5.1. Non-homogenous Solution.....	32
2.5.2. Constant Temperature Distribution ( $T = T_0$ ).....	32
2.5.3. Linear Temperature Distribution ( $T = \lambda(b - r)$ ).....	33
2.5.4. Parabolic Temperature Distribution ( $T = \lambda(b^2 - r^2)$ ).....	34
2.6. Hoffman Failure Criteria.....	36
NUMERICAL RESULTS AND DISCUSSIONS.....	40
3.1 Plane Strain.....	40
3.2 Pressure Vessel.....	51
3.3. Free-End Case.....	59
3.4. Optimum Winding Angle Determination.....	69
CONCLUSION AND FUTURE RECOMMENDATIONS.....	71
REFERENCES.....	73

## LIST OF FIGURES

2.1	Representation of cartesian, cylindrical and material coordinates	11
2.2	Representation of cylindrical coordinates	16
2.3	Matrix and fiber directions	17
2.4	The tube modeled as plane strain case subjected to internal pressure	18
2.5	Linear temperature distribution on the cross-section of the tube	22
2.6	Parabolic temperature distribution on the cross-section of the tube	24
2.7	Boundary conditions of a 4-layered tube subjected to internal pressure	26
2.8	Tube with free ends to expansion	29
2.9	Pressure vessel subjected to internal pressure	29
2.10	Cross section of a pressure vessel	30
3.1	Fail pressure of a vessel with [45°/-45°] for parabolic temperature distribution	41
3.2	The stress distribution at P=5MPA, T=0°C	42
3.3	The stress distribution at P=5MPA, T=42°C	43
3.4	The stress distribution at P=8MPA, T=0°C for moisture concentration of $3 \cdot 10^{-3}$	44
3.5	Fail pressure of a vessel with [45°/-45°] for linear temperature distribution	46
3.6	Fail pressure of a vessel with [45°/-45°] for constant temperature distribution	47
3.7	Fail pressure of a vessel with [60°/-60°] for parabolic temperature distribution	48
3.8	Fail pressure of a vessel with [60°/-60°] for linear temperature distribution	48

3.9	Fail pressure of a vessel with [60°/-60°] for constant temperature distribution	49
3.10	Fail pressure of a vessel with [30°/-30°] for parabolic temperature distribution	49
3.11	Fail pressure of a vessel with [30°/-30°] for linear temperature distribution	50
3.12	Fail pressure of a vessel with for [30°/-30°] for constant temperature distribution	51
3.13	Fail pressure of a pressure vessel with [45°/-45°] for parabolic temperature distribution	51
3.14	The stress distribution for $c=3*10^{-3}$	52
3.15	The stress distribution for $c=10*10^{-3}$	53
3.16	The stress distribution for $c=20*10^{-3}$	54
3.17	The stress distribution at $P=1\text{MPA}, T=0^{\circ}\text{C}$	55
3.18	The stress distribution at $P=7\text{MPA}, T=0^{\circ}\text{C}$	55
3.19	Fail pressure of a pressure vessel with [45°/-45°] for linear temperature distribution	56
3.20	Fail pressure of pressure vessel with [60°/-60°] for parabolic temperature distribution	57
3.21	Fail pressure of a pressure vessel with [60°/-60°] for linear temperature distribution	57
3.22	Fail pressure of a pressure vessel with [30°/-30°] for parabolic temperature distribution	58
3.23	Fail pressure of a pressure vessel with [30°/-30°] for linear temperature distribution	59
3.24	Fail pressure of a vessel with [45°/-45°] for parabolic temperature distribution	60
3.25	The stress distribution for the moisture concentration of $3*10^{-3}$	61
3.26	The stress distribution for the moisture concentration of $10*10^{-3}$	61
3.27	The stress distribution for the moisture concentration of $20*10^{-3}$	62
3.28	The stress distribution at $P=0\text{MPA}, T=66^{\circ}\text{C}$	63

3.29	The stress distribution at P=1MPa, T=0°C	64
3.30	The stress distribution at P=6MPa, T=0°C	65
3.31	Fail pressure of a vessel with [45°/-45°] for linear temperature distribution	65
3.32	Fail pressure of vessel with [60°/-60°] for parabolic temperature distribution	66
3.33	Fail pressure of vessel with free ends for [60°/-60°] for linear temperature distribution	67
3.34	Fail pressure of vessel with [30°/-30°] for parabolic temperature distribution	68
3.35	Fail pressure of vessel with [30°/-30°] for linear temperature distribution	68
3.36	Hoffman index comparison for different winding angles	69

## LIST OF TABLES

3.1	The stress distribution at P=5MPa, T=0°C	42
3.2	The stress distribution at P=5MPa, T=42°C	43
3.3	The stress distribution at P=8MPa, T=0°C for moisture concentration of $3 \times 10^{-3}$	44
3.4	The stress distribution for moisture concentration of $5 \times 10^{-3}$	45
3.5	The stress distribution for moisture concentration of $10 \times 10^{-3}$	45
3.6	Fail temperatures for various moisture concentrations	46
3.7	The stress distribution for $c=3 \times 10^{-3}$	52
3.8	The stress distribution $c=10 \times 10^{-3}$	53
3.9	The stress distribution for $c=20 \times 10^{-3}$	53
3.10	Fail temperatures for various moisture concentrations	54
3.11	The stress distribution at P=1MPa, T=0°C	54
3.12	The stress distribution at P=7MPa T=0°C	55
3.13	Fail pressure of a pressure vessel with [45°/-45°] for constant temperature distribution	56
3.14	Fail pressure of a pressure vessel with [60°/-60°] for constant temperature distribution	58
3.15	Fail pressure of a pressure vessel with [30°/-30°] for constant temperature distribution	59
3.16	The stress distribution for $c=3 \times 10^{-3}$	60
3.17	The stress distribution for $c=10 \times 10^{-3}$ P=7MPa, temperature T=0°Celsius.	61
3.18	The stress distribution for $c=20 \times 10^{-3}$	62
3.19	Fail temperatures of a tube for various moisture concentrations	62
3.20	The stress distribution at T=66°C	63

3.21	The stress distribution at P=1MPa, T=0°C	64
3.22	The stress distribution at P=6MPa, T=0°C	64
3.23	Fail pressure of vessel with [45°/-45°] for constant temperature distribution	66
3.24	Fail pressure of vessel with [60°/-60°] for constant temperature distribution	67
3.25	Fail pressure of vessel with [30°/-30°] for constant temperature distribution	69
3.26	The stress distribution at $\theta = 51^\circ$	70

## LIST OF SYMBOLS

$x, y, z$	Rectangular coordinates
$r, \theta, z$	Cylindrical coordinates
1,2,3	Principal material coordinates
$\sigma_{ij}$	Stress components in rectangular, cylindrical or material coordinates
$\varepsilon_{ij}$	Strain components in rectangular, cylindrical or material coordinates
$C_{ij}$	Stiffness matrix $i, j=1,2,\dots,6$
$u, v, w$	Displacements in $x, y, z$ directions, respectively
$E_{ij}$	Modulus of elasticity in rectangular, cylindrical or material coordinates
$G_{ij}$	Modulus of rigidity in rectangular, cylindrical or material coordinates
$\nu_{ij}$	Poisson's ratio in rectangular, cylindrical or material coordinates
$\bar{U}$	Body Force potential
$F(r, \theta)$	Stress function
$a_{ij}$	Compliance matrix
M	Torque
$\alpha_{z,\theta,r}$	Thermal expansion coefficients in cylindrical coordinates
$\alpha_{1,2}$	Thermal expansion coefficients in fiber and matrix direction
$\beta_{z,\theta,r}$	Moisture expansion coefficients in cylindrical coordinates
$\beta_{1,2}$	Moisture expansion coefficients in fiber and matrix direction
$c$	Moisture concentration
$T$	Temperature
$r$	Radius
$t$	Thickness of one layer
H	Hoffman index

$R$	Resultant Force in z-direction
$P_i$	Inner pressure
$X_T$	Ultimate tensile strength in fiber direction
$X_C$	Ultimate compressive strength in fiber direction
$Y_T$	Ultimate tensile strength in matrix direction
$Y_C$	Ultimate compressive strength in matrix direction
$Z_T$	Ultimate tensile strength in transverse direction
$Z_C$	Ultimate compressive strength in transverse direction

## CHAPTER 1

### INTRODUCTION

A composite material is defined as a combination of two or more materials on a macroscopic scale to form a useful third material. The advantage of composite materials is that they usually exhibit the best qualities of their components and often some qualities that neither their components possesses. The main objective with composite material is to create a material that has only the designed characteristic required to perform the design task. A composite material contains reinforcements supported by a matrix material. Reinforcement can be implemented by fibers or particles. The fibers usually have high strength than the matrix. The matrix has the functionality to keep the fibers in desired position and orientation. Some of the properties that can be improved with a composite material are strength, stiffness, corrosion resistance, strength-to-weight ratio, stiffness-to-weight ratio, low specific gravities, fatigue damage tolerance, noncorrosive behavior, chemical resistance and temperature dependent behavior, impact resistance. In recent years because of these features and with the development of manufacturing technologies, of composites became widespread in many parts of the industry such as aerospace industry, marine, sport applications and automotive industry.

#### 1.1. Fiber Reinforced Composite Materials

Composite materials can be classified according to the physical properties as:

- **Fibrous** composite materials that consist of fibers in a matrix
- **Laminated** composite materials that consist of layers of various materials
- **Particulate** composite materials that are composed of particles in a matrix

- **Combinations** of some or all of the first three types

### 1.1.1. Fibrous Composite Materials

Fibrous composites consist of fibers in a matrix. They are common since long fibers in various forms are much stiffer and stronger than the material in the bulk form. The fibers have different properties from the bulk form because of the perfect structure of fibers, since the crystals are aligned along the fiber axis and there are fewer internal defects in fibers than in bulk material.

### 1.1.2. Mechanical Behavior of Composite Materials

Composite materials have mechanical behavior characteristics that are different from those of more conventional engineering materials. Some characteristics are merely modifications of conventional behavior; others are totally new and require new analytical experimental procedures [3].

Most common engineering materials are both *homogeneous* and *isotropic*:

A *homogeneous* body has uniform properties throughout, i.e., the properties are independent of position in the body.

An *isotropic* body has material properties that are the same in every direction at a point in the body, i.e., the properties are independent of orientation at a point in the body.

Bodies with temperature-dependent isotropic material properties are not homogeneous when subjected to a temperature gradient, but still are isotropic.

In contrast, composite materials are often both *inhomogeneous* and *nonisotropic* (orthotropic or, more generally anisotropic):

An *inhomogeneous* body has nonuniform properties over the body, i.e., the properties depend on position in the body.

An *orthotropic* body has material properties that are different in three mutually perpendicular directions at a point in the body and, further, has three mutually perpendicular planes of material property symmetry. Thus, the properties depend on orientation at a point in the body.

An *anisotropic* body has material properties that are different in all directions at a point in the body. No planes material property symmetry exists. Again, the properties depend on the orientation at a point in the body.

Because of the inherently heterogeneous nature of composite materials, they are conveniently studied from two points of the view: micromechanics and macromechanics.

Use of the two concepts of macromechanics and micromechanics allows the tailoring of a composite material to meet a particular structural requirement with little waste of material capability. The ability to tailor a composite material to its job is one of the most significant advantages of a composite material over an ordinary material. Perfect tailoring of a composite material yields one of the stiffness and strength required in each direction, no more. In contrast, an isotropic material is, by definition, constrained to have excess strength and stiffness in any direction other than that of the largest required strength and stiffness.

The inherent anisotropy (most often only orthotropy) of composite materials leads to mechanical behavior characteristics that are quite different from those conventional isotropic materials.

For isotropic materials, application of normal stress causes extension in the direction of the stress and contraction in the perpendicular directions, but no shearing deformation. Also, application of shear stress causes only shearing deformation, but no extension or contraction in any direction. Only two material properties, Young's modulus and Poisson's ratio, are needed to quantify the deformations. The shear modulus could be used as an alternative to either Young's modulus or Poisson's ratio.

For orthotropic materials, like isotropic materials, application of normal stress in a principal material direction results in extension in the direction of the stress and contraction perpendicular to the stress. The magnitude of the extension in one principal material direction under normal stress in that direction is different from the extension in another principal material direction under the same normal stress in that direction. Thus, different Young's moduli exist in the various principal material directions. In addition, because of different properties in the two principal material directions, the contraction can be either more or less than the contraction of a similarly loaded isotropic material with the same elastic modulus in the direction of

the load. Thus different Poisson's ratios are associated with different pairs of principal material directions (and with the order of the coordinate direction numbers designating the pairs). Application of shear stress causes shearing deformations, but the magnitude of the shearing deformation is totally independent of the various Young's moduli and Poisson's ratio. That is, the shear modulus of an orthotropic material is, unlike isotropic materials, not dependent on other material properties. Thus, at least five material properties are necessary to describe the mechanical behavior of orthotropic materials.

For anisotropic materials, application of a normal stress leads not only to extension in the direction of the stress and contraction perpendicular to it, but to shearing deformation. Conversely, application of shearing stress causes extension and contraction in addition to the distortion of shearing deformation. This coupling between both loading modes and both deformation modes, i.e., shear-extension coupling, is also characteristic of orthotropic materials subjected to normal stress in a non-principal material direction. Even more material properties than for orthotropic materials are necessary to describe the mechanical behavior of anisotropic materials because of the additional response characteristics.

## **1.2. Manufacturing of Fiber-Reinforced Composite Materials**

Unlike most conventional materials, there is a very close relation between the manufacturing of a composite material and its mechanical properties. Hand lay-up technique was the first manufacturing technique. The open mold process with spray-up of chopped fibers was also used for development of work, prototype fabrication and production of large components and relatively small quantities.

A major breakthrough in composite manufacturing technology occurred with the development of "prepreg tape", which is a tape consisting of fibers precoated with the polymer resin. Most prepreg tape is made by the hot-melt process. Autoclave molding is the standard process for fabrication with prepreg tapes.

Sheet-molding compound (SMC) is an important innovation in composite manufacturing.

Nowadays, in addition to these techniques, new production techniques are developed. These are pultrusion, reinforced reaction injection molding,

thermoplastic molding, resin transfer molding, structural reaction injection molding and filament winding.

### **1.3. Filament Winding**

Filament winding is widely used to produce such structures as rocket motor cases, pressure vessels, shafts, piping and tubing.

Filament winding, which involves winding of resin-coated fibers onto a rotating mandrel, may be used to produce any composite structure, which has the form of a body of revolution.

Another advantage of this process is that by controlling the winding tension on fibers, they can be packed together very tightly to produce high fiber volume fractions.

### **1.4. Analysis of Hygrothermal Behavior of Composite Materials**

Many researches have been performed for the prediction of mechanical behavior of composite structures. The determination of mechanical properties of the composite materials, the stress and strain analysis of composite structures, the failure analysis, the structural optimization of the composite structures are the basic aims of the studies. In addition to these, some experiments were also made to verify analytical models developed.

*Lekhnitskii* [2] made a deep investigation on Composite cylinders under internal pressure, twisting moment, axial load or bending moment.

*L. Parnas* and *E. Ahçı* [4] investigated fiber reinforced composite rocket motor case and presented a method to analyze and improve the composite structure, which is subjected to various load. The analysis method can also be applied to composite pressure vessels, storage tanks, and cylinders. The aim of this study is to develop an analytical method that determines the mechanical behavior of the composite structure under combined mechanical (internal and moisture changes) loads. The optimum winding angle that provides the maximum strength to the composite structure and the burst pressure for a certain loading condition and given geometry were also be calculated by this method. The improvement of the composite

structure on the basis of winding angle was made by utilizing the 3-D Quadratic failure in the strain space. A user-friendly computer program running under Microsoft Windows and using the results of this study was developed in Microsoft Visual Basic 4.0 Language for analysis and design purposes. The results obtained were also compared with the experimental findings.

*L. Parnas* and *S. Aleçakır* [5] obtained explicit analytical solutions for the stresses and displacements in each orthotropic layer of a multi-layered filament-wound tube subjected to axi-symmetric loads and bending separately that is based on anisotropic elasticity theory. An experimental study has also been carried out for investigating the bending behavior of composite tubes. A special bending test setup has been designed, produced and bending tests have been performed on 120 sample composite tubes manufactured with a combination of two different fiber types: carbon and glass; two different type of resin systems: two epoxies with different glass transition temperatures; two different diameters and four different winding angles. Using the results of the experiments, a database has been formed for design purposes. The experiments have also been simulated by utilizing the analysis and comparison have been made between the experimental and the theoretical results. The stress-analysis performed has been combined with a suitable, interactive, stress-based macroscopic failure criterion and a good-fitting correlation based on the laminated plate theory for estimating the through thickness elastic constants, to enable the safe design of filament-wound composite tubes under combined loading.

*L. Parnas* and *N. Katırcı* [6] developed an analytical procedure to design and predict the behavior of the reinforced composite pressure vessels. The classical lamination theory and generalized plane strain model is used in the formulation of the elasticity problem. Internal pressure, axial force and body force due to rotation in addition to temperature and moisture variation throughout the body are considered. Some 3D failure theories are applied to obtain the optimum values for the winding angle, burst pressure, maximum axial force and the maximum angular speed of the pressure vessel. These parameters are also investigated considering hygrothermal effects.

*M. Xia*, *H. Takayanagi* and *K. Kemmochi* [7] investigated multi-layered filament-wound (FW) structures. Each layer of the pipes is assumed to be anisotropy. Based on the three-dimensional (3-D) anisotropic elasticity, an exact elastic solution for

stresses and deformations of the pipes under internal pressure is presented. Moreover, detailed stress and strain distributions for three given angle-ply pipe designs are investigated by using the present theory. The shear extension coupling is also considered because the lay-up angles with  $+\Phi$  and  $-\Phi$  layers cannot exist in the same radius. For cylindrical-pressure vessels with different angle-ply pipe, the ratio of applied hoop-to-axial stress in each layer is different. Even if quite a thin-walled pipes, the ratio of hoop-to-axial stress is no longer a constant of 2:1.

*P. M. Wild* and *G. W. Vickers* [8] developed an analytical procedure to assess to stresses and deformations of filament-wound structures under loading conditions particular to centrifuge rotors and to assess the effects of winding angle variation through the centrifuge wall. This procedure is based on classical laminated plate theory and models both plane stress and plane strain states of cylindrical shell comprising a number of cylindrical sublayers, each of which is cylindrically orthotropic. Available loading conditions are: radial body force due to rotation about the cylinder axis, internal and external pressures and axial force. The analysis is applied to three examples: a pressure vessel, a centrifuge rotor and a flywheel. It is shown that the benefit of winding angle variation is more significant for applications in which there is no axial loading to cylindrical shell. It is also shown that, where axial loading is present, the benefits of wind angle variation are more significant under the last ply failure criterion than under the first ply failure criterion.

Based on the curved composite-beam and multilayer-buildup theories, *M. Xia*, *H. Takayanagi*, *K. Kemmochi* [9] presented two methods to analyze the stresses and deflections of multi-ply cylindrical pipes under transverse loading conditions. According to the presented solutions, numerical results are given for a common sandwich type. Stress distributions within a pipe and deflections are also discussed. Simple analytical methods can be used to evaluate the stresses and deflections of multiple-layer cylindrical structures under transverse loading conditions. The results of the experimental investigations of a sandwich pipe are compared to the results of the theoretical calculations. The values obtained from the experimental results fall between the values obtained when each theory is applied separately.

Another work by *M. Xia*, *K. Kemmochi*, *H. Takayanagi* [10] is a presentation based on the classical laminated-plate theory of an elastic solution for the thermal stress

and strain in a filament-wound fiber-reinforced sandwich pipe subjected to internal pressure and temperature change. The sandwich pipe is created using resin material for the core layer and reinforced materials with an alternate-ply for the skin layers. Considering the complicated material properties of the skin layers reinforced by alternate-ply composites, the thermal stress analysis is based on treating typical sandwich pipes that are three-dimensional, cylindrical, and orthotropic. A computer program was developed to conduct stress and deformations analysis of sandwich pipe with different winding angles. Moreover, an optimum winding angle of the filament-wound fiber-reinforced materials was designed by using a netting approach analysis.

*Jiann-Quo Tarn, Yung-Ming Wang* [11] presented a state approach to extension, torsion, bending, shearing and pressuring of laminated composite tubes. One of the novel features is that they have formulated the basic equations of an anisotropic elasticity in the cylindrical coordinate system into a state equation by a judicious arrangement of the displacement and stress variables so that the system matrix is independent of  $r$ . The formulation suggests a systematic way using matrix algebra and the transverse matrix is determine the stress and deformation in a multilayered cylindrically anisotropic tube under applied loads that do not vary in the axial direction. An exact analysis of the tube subjected to uniform surface tractions, an axial force, a torque and bending moments is presented. The solution consists of an axisymmetric state due to extension, torsion, uniform pressuring and shearing, and an asymmetric state due to bending. The formalism indicates that extension, torsion and pressuring interact; uniform shearing causes pure shears in the laminated tube, regardless of the number of layers. These deformations are uncoupled with bending of the tube.

*Cho-Chung Liang, Hung-Wen Chen, Cheng-Huan Wang* [12] investigated the optimum design of dome contours for filament-wound composite pressure vessels, subjected to geometrical limitations, winding condition, and the Tsai-Wu criterion and maximizing shape factor, the feasible direction method being employed. An actual design example, presented by Fukunaga is adapted to the study the optimum dome contour using the present method. Results reveal that the dome contours using the present method, Fukunaga's method and the netting method can be approximated using elliptic curves, and that the depth is the major parameter for

optimizing the design of dome contour, and the dome, designed using the present methods has stronger structure and greater internal volume than those designed using other approaches. Results reveal that the present method is usable for the optimum design of dome contours for filament-wound composite pressure vessels.

In this study, a method for analyzing fiber reinforced composite vessels under hygrothermal loading has been developed. For this, an explicit analytical formulation is developed based on the anisotropic elasticity theory that determines the behavior of the vessel under thermal and moisture effects.

In the present study, stress analysis and as a result of this stress analysis, failure analysis were investigated in multiple layered composite cylinders under internal pressure and hygrothermal loads. The solution was carried out analytically. The elastic formulation was obtained for a layer. Then, it was evaluated for  $n$  layers. In the solution, the integral constants are determined by using the boundary conditions in a matrix form. This method can be applied to all long composite cylinders, pressure vessels and tanks. After finding analytical solution, two different computer programs are developed to find the behavior of the tube under hygrothermal loading conditions.

## **CHAPTER2**

### **THEORETICAL ANALYSIS**

#### **2.1. Introduction**

In general, composite materials are used in the form of laminates. In order to understand the physical behavior of composite cylinders, pressure vessels and rocket motor cases, it is necessary to review the theory of anisotropic elasticity. In this chapter, the developed analytical procedure is explained in detail starting from the equations of anisotropic elasticity.

#### **2.2. Constitutive Relationships for an Orthotropic Lamina**

The stress-strain relations in the principal material directions 1,2 and 3 for a single unidirectional fiber-reinforced lamina, in a linear orthotropic material, are given in the matrix (2.1), where direction 1 is the fiber directions and 2, 3 are perpendicular to the fibers. Direction 1 and 2 are in plane and direction 3 is in the trough-thickness direction as presented in the figure 2.1.

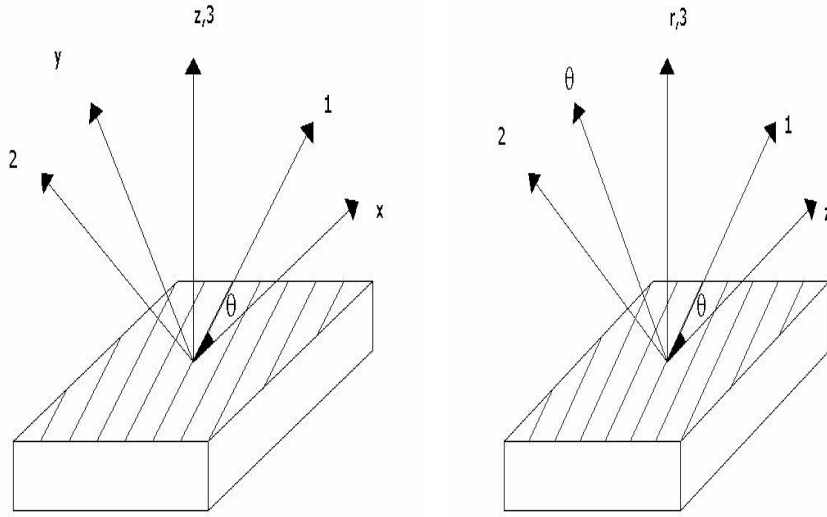


Figure 2.1. Representation of cartesian, cylindrical and material coordinates

All the elastic constants including the through-thickness constants have been determined by hypothetical tests. In these tests, each layer of filament-wound tube is modeled as a balanced angle-ply.

Equations representing the Generalized Hook's Law in the principal (material directions) 1,2 and 3 for a single orthotropic unidirectional fiber-reinforced lamina (using row-normalized elastic constants) are as follows

$$\begin{Bmatrix} \varepsilon_{11} \\ \varepsilon_{22} \\ \varepsilon_{33} \\ \gamma_{23} \\ \gamma_{13} \\ \gamma_{12} \end{Bmatrix} = \begin{bmatrix} \frac{1}{E_{11}} & -\frac{\nu_{12}}{E_{11}} & -\frac{\nu_{13}}{E_{11}} & 0 & 0 & 0 \\ -\frac{\nu_{21}}{E_{22}} & \frac{1}{E_{22}} & -\frac{\nu_{23}}{E_{22}} & 0 & 0 & 0 \\ -\frac{\nu_{31}}{E_{33}} & -\frac{\nu_{32}}{E_{33}} & \frac{1}{E_{33}} & 0 & 0 & 0 \\ 0 & 0 & 0 & \frac{1}{G_{23}} & 0 & 0 \\ 0 & 0 & 0 & 0 & \frac{1}{G_{13}} & 0 \\ 0 & 0 & 0 & 0 & 0 & \frac{1}{G_{12}} \end{bmatrix} \begin{Bmatrix} \sigma_{11} \\ \sigma_{22} \\ \sigma_{33} \\ \tau_{23} \\ \tau_{13} \\ \tau_{12} \end{Bmatrix} \quad (2.1)$$

When the compliance matrix above is inverted, the stress-strain equations become

$$\begin{Bmatrix} \sigma_1 \\ \sigma_2 \\ \sigma_3 \\ \tau_{23} \\ \tau_{13} \\ \tau_{12} \end{Bmatrix} = \begin{bmatrix} C_{11} & C_{12} & C_{13} & 0 & 0 & 0 \\ C_{21} & C_{22} & C_{23} & 0 & 0 & 0 \\ C_{31} & C_{32} & C_{33} & 0 & 0 & 0 \\ 0 & 0 & 0 & C_{44} & 0 & 0 \\ 0 & 0 & 0 & 0 & C_{55} & 0 \\ 0 & 0 & 0 & 0 & 0 & C_{66} \end{bmatrix} \begin{Bmatrix} \varepsilon_1 \\ \varepsilon_2 \\ \varepsilon_3 \\ \gamma_{23} \\ \gamma_{13} \\ \gamma_{12} \end{Bmatrix} \quad (2.2)$$

The coefficients  $C_{ij}$  ( $i, j = 1, 2, \dots, 6$ ) are the stiffness of the composite material and defined as follows, in terms of the engineering constants

$$\begin{aligned} C_{11} &= (1 - \nu_{23}\nu_{32})VE_1 \\ C_{12} &= C_{21} = (\nu_{21} + \nu_{23}\nu_{31})VE_1 \\ C_{13} &= C_{31} = (\nu_{31} + \nu_{32}\nu_{21})VE_1 \\ C_{22} &= (1 - \nu_{13}\nu_{31})VE_2 \\ C_{23} &= C_{32} = (\nu_{32} + \nu_{31}\nu_{12})VE_2 \\ C_{33} &= (1 - \nu_{12}\nu_{21})VE_3 \\ C_{44} &= G_{23} \\ C_{55} &= G_{13} \\ C_{66} &= G_{12} \end{aligned} \quad (2.3)$$

where

$$V = \frac{1}{1 - \nu_{12}\nu_{21} - \nu_{13}\nu_{31} - \nu_{23}\nu_{32} - 2\nu_{21}\nu_{13}\nu_{32}}$$

When the stresses are transformed from the material directions 1, 2, 3 to loading directions x, y, z (Fig 2.1) by rotating through an angle  $\theta$  about the z-axis, then the matrix in equation (2.4) is obtained

$$\begin{Bmatrix} \sigma_{xx} \\ \sigma_{yy} \\ \sigma_{zz} \\ \tau_{yz} \\ \tau_{xz} \\ \tau_{xy} \end{Bmatrix} = \begin{bmatrix} \bar{C}_{11} & \bar{C}_{12} & \bar{C}_{13} & 0 & 0 & \bar{C}_{16} \\ \bar{C}_{21} & \bar{C}_{22} & \bar{C}_{23} & 0 & 0 & \bar{C}_{26} \\ \bar{C}_{31} & \bar{C}_{32} & \bar{C}_{33} & 0 & 0 & \bar{C}_{36} \\ 0 & 0 & 0 & \bar{C}_{44} & \bar{C}_{45} & 0 \\ 0 & 0 & 0 & \bar{C}_{45} & \bar{C}_{55} & 0 \\ \bar{C}_{16} & \bar{C}_{26} & \bar{C}_{36} & 0 & 0 & \bar{C}_{66} \end{bmatrix} \begin{Bmatrix} \varepsilon_{xx} \\ \varepsilon_{yy} \\ \varepsilon_{zz} \\ \gamma_{yz} \\ \gamma_{xz} \\ \gamma_{xy} \end{Bmatrix} \quad (2.4)$$

where the elements of the transformed stiffness matrix having fibers at an angle  $+\alpha$  to the loading direction, are obtained as follows

$$\begin{aligned} \bar{C}_{11} &= m^4 C_{11} + 2m^2 n^2 (C_{12} + 2C_{66}) + n^4 C_{22} \\ \bar{C}_{12} &= m^2 n^2 (C_{11} + C_{22} - 4C_{66}) + (m^4 + n^4) C_{12} \\ \bar{C}_{13} &= m^2 C_{13} + n^2 C_{23} \\ \bar{C}_{16} &= -mn^3 C_{22} + m^3 n C_{11} - mn(m^2 - n^2)(C_{12} + 2C_{66}) \\ \bar{C}_{22} &= n^4 C_{11} + 2m^2 n^2 (C_{12} + 2C_{66}) + m^4 C_{22} \\ \bar{C}_{23} &= n^2 C_{13} + m^2 C_{23} \\ \bar{C}_{26} &= -m^3 n C_{22} + mn^3 C_{11} + mn(m^2 - n^2)(C_{12} + 2C_{66}) \\ \bar{C}_{33} &= C_{33} \\ \bar{C}_{36} &= mn(C_{13} - C_{23}) \\ \bar{C}_{44} &= m^2 C_{44} + n^2 C_{55} \\ \bar{C}_{45} &= mn(C_{55} - C_{44}) \\ \bar{C}_{55} &= m^2 C_{55} + n^2 C_{44} \\ \bar{C}_{66} &= m^2 n^2 (C_{11} + C_{22} - 2C_{12}) + (m^2 - n^2) C_{66} \end{aligned} \quad (2.5)$$

where  $m = \cos(\alpha)$  and  $n = \sin(\alpha)$ .

The effective through thickness elastic constants for the laminate, which actually correspond to the transformed elastic coefficients for any layer of a filament-wound tube, can be found from the hypothetical tests by evaluating the stress resultants in terms of the above coefficients. The elastic constants for a laminate are

$$\begin{aligned}
E_{xx} &= \frac{\bar{C}_{11}\bar{C}_{22}\bar{C}_{33} - \bar{C}_{11}\bar{C}_{23}\bar{C}_{23} - \bar{C}_{22}\bar{C}_{13}\bar{C}_{13} - \bar{C}_{33}\bar{C}_{12}\bar{C}_{12} + 2\bar{C}_{23}\bar{C}_{31}\bar{C}_{12}}{\bar{C}_{22}\bar{C}_{33} - \bar{C}_{23}\bar{C}_{23}} \\
E_{yy} &= \frac{\bar{C}_{11}\bar{C}_{22}\bar{C}_{33} - \bar{C}_{11}\bar{C}_{23}\bar{C}_{23} - \bar{C}_{22}\bar{C}_{13}\bar{C}_{13} - \bar{C}_{33}\bar{C}_{12}\bar{C}_{12} + 2\bar{C}_{23}\bar{C}_{31}\bar{C}_{12}}{\bar{C}_{11}\bar{C}_{33} - \bar{C}_{13}\bar{C}_{13}} \\
E_{zz} &= \frac{\bar{C}_{11}\bar{C}_{22}\bar{C}_{33} - \bar{C}_{11}\bar{C}_{23}\bar{C}_{23} - \bar{C}_{22}\bar{C}_{13}\bar{C}_{13} - \bar{C}_{33}\bar{C}_{12}\bar{C}_{12} + 2\bar{C}_{23}\bar{C}_{31}\bar{C}_{12}}{\bar{C}_{11}\bar{C}_{22} - \bar{C}_{12}\bar{C}_{12}} \\
G_{yz} &= \bar{C}_{44} \\
G_{xz} &= \bar{C}_{55} \\
G_{xy} &= \frac{\bar{C}_{33}\bar{C}_{66} - \bar{C}_{36}\bar{C}_{36}}{\bar{C}_{33}} \\
\nu_{xy} &= \frac{\bar{C}_{12}\bar{C}_{33} - \bar{C}_{13}\bar{C}_{23}}{\bar{C}_{22}\bar{C}_{33} - \bar{C}_{23}\bar{C}_{23}} \\
\nu_{yx} &= \frac{\bar{C}_{12}\bar{C}_{33} - \bar{C}_{13}\bar{C}_{23}}{\bar{C}_{11}\bar{C}_{33} - \bar{C}_{13}\bar{C}_{13}} \\
\nu_{zx} &= \frac{\bar{C}_{13}\bar{C}_{22} - \bar{C}_{12}\bar{C}_{23}}{\bar{C}_{11}\bar{C}_{22} - \bar{C}_{12}\bar{C}_{12}} \\
\nu_{xz} &= \frac{\bar{C}_{13}\bar{C}_{22} - \bar{C}_{12}\bar{C}_{23}}{\bar{C}_{22}\bar{C}_{33} - \bar{C}_{23}\bar{C}_{23}} \\
\nu_{zy} &= \frac{\bar{C}_{11}\bar{C}_{23} - \bar{C}_{12}\bar{C}_{13}}{\bar{C}_{11}\bar{C}_{22} - \bar{C}_{12}\bar{C}_{12}} \\
\nu_{yz} &= \frac{\bar{C}_{11}\bar{C}_{23} - \bar{C}_{12}\bar{C}_{13}}{\bar{C}_{11}\bar{C}_{33} - \bar{C}_{13}\bar{C}_{13}}
\end{aligned} \tag{2.6}$$

At this point, noting that the angle ply is part of any layer of a filament wound tube where  $x$  axis of the  $x$ - $y$ - $z$  loading axis coincides with the  $z$ -axis of the tube, in order to switch to the tube coordinates, a change of subscripts shown below, which is actually equivalent to a positive rotation of  $90^\circ$  about the  $r$ -axis of a  $\theta$ - $z$ - $r$  coordinate system is enough:

$$x \rightarrow z$$

$$y \rightarrow \theta$$

$$z \rightarrow r$$

The winding angle and the stresses are dependent of the sign of  $\alpha$ , but the elastic constants are not. Since each layer of the filament-wound tube is composed of two sub layers of  $+\alpha$  and  $-\alpha$ , before failure prediction, the stresses for these sub-layers should be separately transformed to the principle material directions.

### 2.3. General Relations

In this section, the governing equations are developed which will be used for three cases investigated in this study. These are plane strain case, free ends and pressure vessel cases. For the most general case, the strain-stress relations can be written in a symmetric matrix formula as

$$\begin{bmatrix} \varepsilon_{rr} \\ \varepsilon_{\theta\theta} \\ \varepsilon_{zz} \\ \gamma_{\theta z} \\ \gamma_{rz} \\ \gamma_{r\theta} \end{bmatrix} = \begin{bmatrix} a_{11} & a_{12} & a_{13} & a_{14} & a_{15} & a_{16} \\ a_{21} & a_{22} & a_{23} & a_{24} & a_{25} & a_{26} \\ a_{31} & a_{32} & a_{33} & a_{34} & a_{35} & a_{36} \\ a_{41} & a_{42} & a_{43} & a_{44} & a_{45} & a_{46} \\ a_{51} & a_{52} & a_{53} & a_{54} & a_{55} & a_{56} \\ a_{61} & a_{62} & a_{63} & a_{64} & a_{65} & a_{66} \end{bmatrix} \begin{bmatrix} \sigma_{rr} \\ \sigma_{\theta\theta} \\ \sigma_{zz} \\ \tau_{\theta z} \\ \tau_{rz} \\ \tau_{r\theta} \end{bmatrix} \quad (2.7)$$

If  $F$ ,  $\Psi$  are the stress functions and  $\bar{U}$  is the potential function respectively, the stress components are derived from reference [2] as

$$\begin{aligned} \sigma_{rr} &= \frac{1}{r} \frac{\partial F(r, \theta)}{\partial r} + \frac{1}{r^2} \frac{\partial^2 F(r, \theta)}{\partial \theta^2} + \bar{U} \\ \sigma_{\theta\theta} &= \frac{\partial^2 F(r, \theta)}{\partial r^2} + \bar{U} \\ \tau_{r\theta} &= -\frac{\partial^2}{\partial r \partial \theta} \left( \frac{F(r, \theta)}{r} \right) \\ \tau_{rz} &= \frac{1}{r} \frac{\partial \Psi}{\partial r} \\ \tau_{\theta z} &= -\frac{\partial \Psi}{\partial r} \end{aligned} \quad (2.8)$$

No body force  $\Rightarrow \bar{U} = 0$

Axially symmetric, therefore  $\frac{\partial^2 F(r, \theta)}{\partial \theta^2} = 0$  and  $\tau_{r\theta} = 0$ ,  $\tau_{rz} = 0$

$\sigma_{rr}$  and  $\sigma_{\theta\theta}$  can be simplified as

$$\sigma_{rr} = \frac{1}{r} \frac{\partial F}{\partial r} \quad (2.9)$$

$$\sigma_{\theta\theta} = \frac{\partial^2 F}{\partial r^2} \quad (2.10)$$

For this problem,  $M=0$ ,  $M$ : Torsional moment

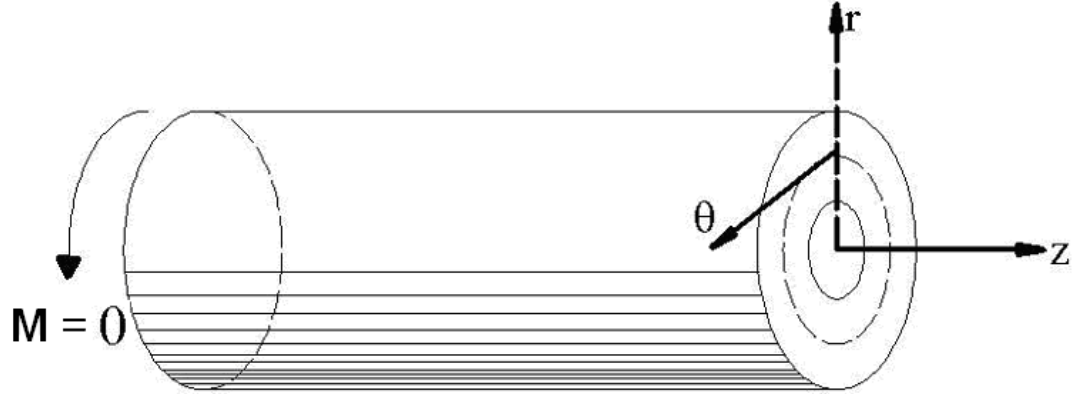


Figure 2.2 Representation of cylindrical coordinates

$$\int_{r=a}^b 2\pi r \tau_{\theta z} r dr = M \Rightarrow \int_a^b 2\pi r^2 \frac{\partial \Psi}{\partial r} dr = M$$

$$\int_a^b 2\pi r^2 \Psi = M \Rightarrow \Psi f(r) = M \quad M=0 \Rightarrow \Psi = 0$$

$$\Rightarrow \tau_{\theta z} = 0$$

This problem is axially symmetric. Moreover from reference [2];

$$a_{12} = a_{21}, \quad a_{23} = a_{32}, \quad a_{13} = a_{31}$$

Hence, the matrix reduces to

$$\begin{bmatrix} \varepsilon_{rr} \\ \varepsilon_{\theta\theta} \\ \varepsilon_{zz} \end{bmatrix} = \begin{bmatrix} a_{11} & a_{12} & a_{13} \\ a_{12} & a_{22} & a_{23} \\ a_{13} & a_{23} & a_{33} \end{bmatrix} \begin{bmatrix} \sigma_{rr} \\ \sigma_{\theta\theta} \\ \sigma_{zz} \end{bmatrix} \quad (2.11)$$

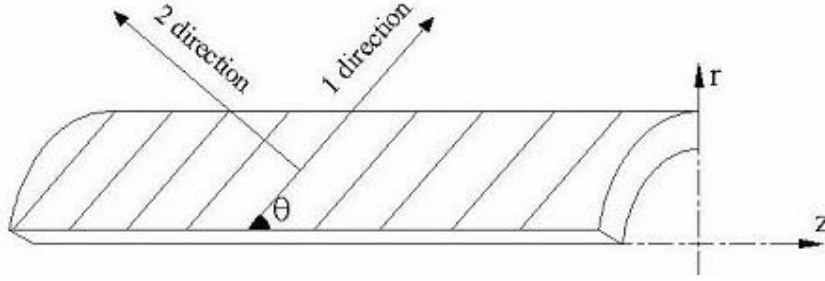


Figure 2.3 Matrix and fiber directions

Strain- displacement equations are defined as

$$\begin{aligned}\varepsilon_{zz} &= \frac{\partial w}{\partial z} \\ \varepsilon_{rr} &= \frac{\partial u}{\partial r} \\ \varepsilon_{\theta\theta} &= \frac{1}{r} \frac{\partial v}{\partial \theta} + \frac{u}{r}\end{aligned}\tag{2.12}$$

Thermal expansion coefficients and hygrothermal expansion coefficients in  $z$  and  $\theta$  directions can be written as

$$\begin{aligned}\alpha_z &= \alpha_1 \cos^2 \theta + \alpha_2 \sin^2 \theta \\ \alpha_\theta &= \alpha_1 \sin^2 \theta + \alpha_2 \cos^2 \theta \\ \beta_z &= \beta_1 \cos^2 \theta + \beta_2 \sin^2 \theta \\ \beta_\theta &= \beta_1 \sin^2 \theta + \beta_2 \cos^2 \theta\end{aligned}\tag{2.13}$$

where  $\alpha_1$ ,  $\alpha_2$  are the thermal expansion coefficients in the principal material direction and  $\beta_1$ ,  $\beta_2$  are the moisture expansion coefficients in the principal material directions.

It is assumed that the material properties in the direction of  $r$  are equal to the material properties in the transverse directions.

After adding hygrothermal effects to mechanical stresses; then the following stress-strain relations are obtained

$$\varepsilon_{rr} = a_{11}\sigma_{rr} + a_{12}\sigma_{\theta\theta} + a_{13}\sigma_{zz} + \alpha_r T + \beta_r c\tag{2.14}$$

$$\varepsilon_{\theta\theta} = a_{12}\sigma_{rr} + a_{22}\sigma_{\theta\theta} + a_{23}\sigma_{zz} + \alpha_\theta T + \beta_\theta c\tag{2.15}$$

$$\varepsilon_{zz} = a_{13}\sigma_{rr} + a_{32}\sigma_{\theta\theta} + a_{33}\sigma_{zz} + \alpha_z T + \beta_z c \quad (2.16)$$

where T is the temperature and c is the moisture concentration, which is defined as the ratio of mass of moisture to mass of dry material in a unit.

### 2.3. Plane Strain Case

Plane strain is the case that the cylinders are closed by two fixed and plane surfaces. Long cylinders, which have very small  $t/L$  ratio, are assumed also as the plane strain problem. Since the tube is prevented to expand by fixed surfaces, the strain in z- direction is equal to zero; therefore the equation (2.16) can be written as

$$\varepsilon_{zz} = a_{13}\sigma_{rr} + a_{32}\sigma_{\theta\theta} + a_{33}\sigma_{zz} + \alpha_z T + \beta_z c = 0 \quad (2.17)$$

From the equation (2.17)  $\sigma_{zz}$  can be found as

$$\sigma_{zz} = \frac{a_{13}}{a_{33}}\sigma_{rr} - \frac{a_{32}}{a_{33}}\sigma_{\theta\theta} - \frac{\alpha_z T}{a_{33}} - \frac{\beta_z c}{a_{33}}$$

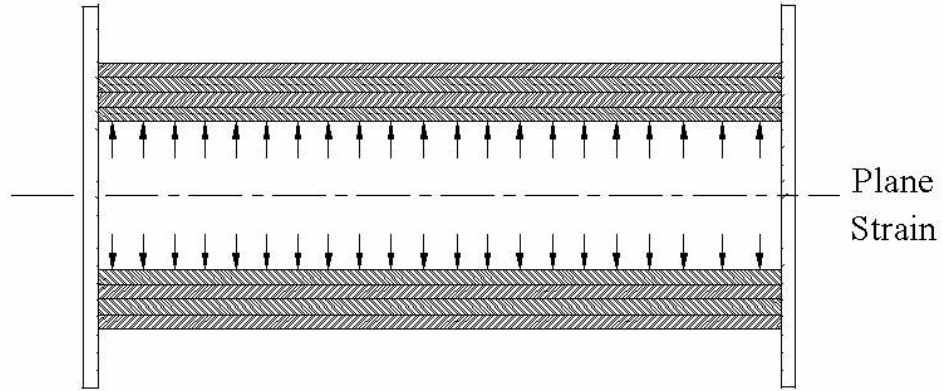


Figure 2.4 the tube modeled as plane strain case subjected to internal pressure

After replacing  $\sigma_{zz}$  in the equations (2.14) and (2.15), then the equations (2.18) and (2.19) are obtained

$$\varepsilon_{rr} = \left(a_{11} - \frac{a_{13}}{a_{33}}a_{13}\right)\sigma_{rr} + \left(a_{12} - \frac{a_{32}}{a_{33}}a_{13}\right)\sigma_{\theta\theta} + \left(\alpha_r - \frac{\alpha_z a_{13}}{a_{33}}\right)T + \left(\beta_r - \frac{\beta_z a_{13}}{a_{33}}\right)c \quad (2.18)$$

$$\varepsilon_{\theta\theta} = \left(a_{12} - \frac{a_{13}}{a_{33}}a_{23}\right)\sigma_{rr} + \left(a_{22} - \frac{a_{23}}{a_{33}}a_{23}\right)\sigma_{\theta\theta} + \left(\alpha_{\theta} - \frac{\alpha_z a_{23}}{a_{33}}\right)T + \left(\beta_{\theta} - \frac{\beta_z a_{23}}{a_{33}}\right)c \quad (2.19)$$

or the equations (2.18) and (2.19) can be written shortly as

$$\varepsilon_{rr} = \beta_{11}\sigma_{rr} + \beta_{12}\sigma_{\theta\theta} + \alpha_{rr}T + \beta_{rr}c \quad (2.20)$$

$$\varepsilon_{\theta\theta} = \beta_{12}\sigma_{rr} + \beta_{22}\sigma_{\theta\theta} + \alpha_{\theta\theta}T + \beta_{\theta\theta}c$$

where  $\beta_{11}$ ,  $\beta_{12}$ ,  $\beta_{22}$ ,  $\alpha_{rr}$ ,  $\alpha_{\theta\theta}$ ,  $\beta_{rr}$  and  $\beta_{\theta\theta}$  are defined as

$$\begin{aligned} \beta_{11} &= a_{11} - \frac{a_{13}^2}{a_{33}}, \quad \beta_{12} = a_{12} - \frac{a_{23}a_{13}}{a_{33}}, \quad \beta_{22} = a_{22} - \frac{a_{23}^2}{a_{33}}, \quad \alpha_{rr} = \alpha_r - \frac{\alpha_z a_{13}}{a_{33}} \\ \beta_{rr} &= \beta_r - \frac{\beta_z a_{13}}{a_{33}}, \quad \alpha_{\theta\theta} = \alpha_{\theta} - \frac{\alpha_z a_{23}}{a_{33}}, \quad \beta_{\theta\theta} = \beta_{\theta} - \frac{\beta_z a_{23}}{a_{33}} \end{aligned} \quad (2.21)$$

If the equation (2.12) is put into the equation (2.20), then the following equation will be obtained

$$\varepsilon_{rr} = \frac{\partial u}{\partial r} = \frac{du}{dr} = \beta_{11}\sigma_{rr} + \beta_{12}\sigma_{\theta\theta} + \alpha_{rr}T + \beta_{rr}c \quad (2.22)$$

Similarly,  $\varepsilon_{\theta\theta}$  can be written as

$$\varepsilon_{\theta\theta} = \frac{1}{r} \frac{\partial v}{\partial \theta} + \frac{u}{r} = \beta_{12}\sigma_{rr} + \beta_{22}\sigma_{\theta\theta} + \alpha_{\theta\theta}T + \beta_{\theta\theta}c \quad (2.23)$$

Since the problem is axially symmetric,  $\frac{\partial v}{\partial \theta} = 0$

If the relations presented in the equation (2.10) are put into the equations (2.22) and (2.23), then these equations can be written as

$$\varepsilon_{rr} = \frac{du}{dr} = \beta_{11} \frac{F'}{r} + \beta_{12}F'' + T\alpha_{rr} + c\beta_{rr} \quad (2.24)$$

$$\varepsilon_{\theta\theta} = \frac{u}{r} = \beta_{12} \frac{F'}{r} + \beta_{22}F'' + T\alpha_{\theta\theta} + c\beta_{\theta\theta} \quad (2.25)$$

The derivative of u in the equation (2.25) should be equal to  $\varepsilon_{rr}$ , given in the

equation (2.24), since  $\varepsilon_{rr} = \frac{du}{dr}$

$$\begin{aligned} \beta_{11} \frac{F'}{r} + \beta_{12}F'' + T\alpha_{rr} + c\beta_{rr} &= \beta_{12} \frac{F'}{r} + \beta_{22}F'' + \beta_{22}rF''' + T\alpha_{\theta\theta} + rT'\alpha_{\theta\theta} + c\beta_{\theta\theta} \quad \text{or} \\ \beta_{22}r^2F''' + \beta_{22}rF'' - \beta_{11}F' &= (\alpha_{rr} - \alpha_{\theta\theta})rT - \alpha_{\theta\theta}r^2T' + (\beta_{rr} - \beta_{\theta\theta})cr \end{aligned} \quad (2.26)$$

Multiplying the equation (2.26) with  $\frac{r}{\beta_{22}}$ , then the equation (2.27) is obtained:

$$r^3 F''' + r^2 F'' - k^2 r F' = \left(\frac{\alpha_{rr} - \alpha_{\theta\theta}}{\beta_{22}}\right) r^2 T - \frac{\alpha_{\theta\theta}}{\beta_{22}} r^3 T' + \left(\frac{\beta_{rr} - \beta_{\theta\theta}}{\beta_{22}}\right) c r^2 \quad (2.27)$$

where  $k$  is defined as  $k = \sqrt{\frac{\beta_{11}}{\beta_{22}}}$

If  $\alpha_{11}$ ,  $\alpha_{22}$  and  $\alpha_{33}$  are defined as

$$\alpha_{11} = \frac{\alpha_{rr} - \alpha_{\theta\theta}}{\beta_{22}}, \quad \alpha_{22} = -\frac{\alpha_{\theta\theta}}{\beta_{22}}, \quad \alpha_{33} = \frac{\beta_{rr} - \beta_{\theta\theta}}{\beta_{22}}$$

Then the equation (2.27) becomes

$$r^3 F''' + r^2 F'' - k^2 r F' = T \alpha_{11} r^2 + T' \alpha_{22} r^3 + c \alpha_{33} r^2 \quad (2.28)$$

The equation (2.28) is the fundamental equation to be solved in the following sections, which includes non-homogenous roots. To solve the homogenous equation,  $r$  should be defined as

$$r = e^t$$

$$\frac{dF}{dr} = \frac{dF}{dt} \frac{dt}{dr} = e^{-t} F'$$

Putting the derivatives of the stress function into the equation (2.28), then the homogenous equation can be written as

$$\begin{aligned} (e^t)^3 (3e^{-3t} F' - 3e^t F'' + e^{-3t} F''') + (e^t)^2 (-e^{-2t} F' + e^{-2t} F'') - k^2 r (e^{-t} F') &= 0 \\ 2F'' - 3F''' + F''' + (-F' + F'') - k^2 F' &= 0 \\ F''' - 2F'' + (1 - k^2) F' &= 0 \end{aligned} \quad (2.29)$$

The roots of the homogeneous equation (2.29) are  $R_1 = 0$ ,  $R_2 = 1 + k$  and  $R_3 = 1 - k$

Then, the homogenous solution is presented as

$$F_h = C_1 + C_2 e^{(1+k)t} + C_3 e^{(1-k)t} \text{ or}$$

$$F_h = C_1 + C_2 r^{(1+k)} + C_3 r^{(1-k)}$$

### 2.3.1 Non-Homogenous Solution

Putting the roots of the homogenous solution into the equation itself, the equation (2.28) becomes:

$$F''' - 2F'' + (1 - k^2)F' = \alpha_{22}T'r^3 + T\alpha_{11}r^2 + c\alpha_{33}r^2 \quad (2.30)$$

In this study, the solution is carried out under the uniform, linear and parabolic temperature distribution. The uniform temperature distribution is usually seen in composite cylinder applications. When the temperature distribution is different in the inner and outer surfaces of the composite cylinder in the steady state case, the temperature function takes a logarithmic form. The parabolic temperature distribution may be seen at any time interval for transient thermal stress cases. For this reason, the solution is also performed under the parabolic temperature distribution.

### 2.3.2. Constant Temperature Distribution ( $T = T_0$ )

Since T is constant, the derivative of T is equal to 0. Then the equation (2.30) becomes

$$F''' - 2F'' + (1 - k^2)F' = (T_0\alpha_{11} + c\alpha_{33})r^2 \quad (2.31)$$

If  $A_1$  is defined as  $A_1 = T_0\alpha_{11} + c\alpha_{33}$ , then the equation (2.31) becomes

$$F''' - 2F'' + (1 - k^2)F' = A_1e^{2t} \quad (2.32)$$

To solve the equation, it is required to define the non-homogenous solution by a coefficient D as

$$F_{NH} = De^{2t}$$

Putting  $F_{NH}$  into the equation (2.32), this equation can be written as

$$8De^{2t} - 8De^{2t} + 2(1 - k^2)De^{2t} = A_1e^{2t} \quad (2.33)$$

Then from the equation (2.33), D is found as

$$D = \frac{A_1}{2(1 - k^2)}$$

Combining the homogeneous and non-homogenous solution, then the stress function becomes

$$F = C_1 + C_2r^{1+k} + C_3r^{1-k} + \frac{A_1}{2(1 - k^2)}r^2 \quad (2.34)$$

Since  $\sigma_{rr} = \frac{F'}{r}$ , as it is presented in the equation (2.9), then  $\sigma_{rr}$  becomes

$$\sigma_{rr} = \frac{F'}{r} = C_2(1+k)r^{k-1} + C_3(1-k)r^{-k-1} + \frac{A_1}{1-k^2} \quad (2.35)$$

and since  $\sigma_{\theta\theta} = F''$  as it is presented in the equation (2.10), then  $\sigma_{\theta\theta}$  becomes

$$\sigma_{\theta\theta} = C_2k(1+k)r^{k-1} - C_3k(1-k)r^{-k-1} + \frac{A_1}{1-k^2}$$

From equation (2.25), u can be found as

$$u = \beta_{12}C_2(1+k)r^k + \beta_{12}C_3(1-k)r^{-k} + \beta_{12}\frac{A_1}{1-k^2}r + \beta_{22}C_2k(1+k)r^k - \beta_{22}C_3k(1-k)r^{-k} + \beta_{22}\frac{A_1}{1-k^2}r + \alpha_{\theta\theta}Tr + \beta_{\theta\theta}cr \quad (2.36)$$

The equations (2.35) and (2.36) will be used as boundary condition to solve the problem. As it can be seen, there are two unknown constants for each layer given by  $C_2$  and  $C_3$ .

### 2.3.3. Linear Temperature Distribution ( $T = \lambda(b-r)$ )

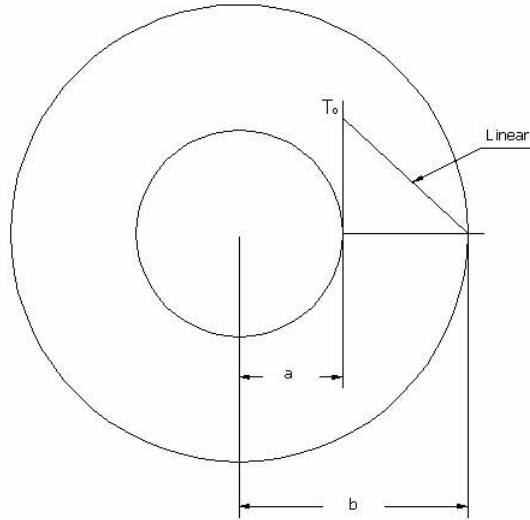


Figure 2.5 Linear temperature distributions on the cross-section of the tube

T is equal to  $T_0$  at the inner surface where  $\lambda$  is defined as  $\lambda = \frac{T_0}{b-a}$ . Thus

$$T' = -\lambda$$

If T is put into the equation (2.30), then this equation becomes

$$F''' - 2F'' + (1-k^2)F' = \alpha_{22}(-\lambda)r^3 + \lambda(b-r)\alpha_{11}r^2 + c\alpha_{33}r^2 \quad \text{or}$$

$$F''' - 2F'' + (1 - k^2)F' = -\lambda(\alpha_{22} + \alpha_{11})r^3 + (\lambda\alpha_{11}b + \alpha_{33}c)r^2 \quad (2.37)$$

If  $A_1$  and  $A_2$  are defined as

$$A_1 = -\lambda(\alpha_{22} + \alpha_{11})$$

$$A_2 = \lambda\alpha_{11}b + \alpha_{33}c$$

Then, the equation (2.37) becomes

$$F''' - 2F'' + (1 - k^2)F' = A_1e^{3t} + A_2e^{2t} \quad (2.38)$$

To solve the non-homogenous equation (2.38), it is required to define two unknown coefficients  $D_1$  and  $D_2$  as

$$F_{NH} = D_1e^{3t} + D_2e^{2t}$$

If  $F_{NH}$  is substituted in the equation (2.38), then this equation becomes

$$27D_1e^{3t} + 8D_2e^{2t} - 18D_1e^{3t} - 8D_2e^{2t} + (1 - k^2)(3D_1e^{3t} + 2D_2e^{2t}) = A_1e^{3t} + A_2e^{2t} \quad (2.39)$$

$D_1$  and  $D_2$  can be found from the equation (2.39) as

$$A_1 = (12 - 3k^2)D_1 \Rightarrow D_1 = \frac{A_1}{3(4 - k^2)}$$

$$A_2 = (2 - 2k^2)D_2 \Rightarrow D_2 = \frac{A_2}{2(1 - k^2)}$$

Then, F becomes

$$F = C_1 + C_2r^{1+k} + C_3r^{(1-k)} + \frac{A_1}{3(4 - k^2)}r^3 + \frac{A_2}{2(1 - k^2)}r^2 \quad (2.40)$$

Therefore the stress components are found as

$$\sigma_{rr} = \frac{F'}{r} = (1 + k)C_2r^{k-1} + (1 - k)C_3r^{-k-1} + \frac{A_1}{4 - k^2}r + \frac{A_2}{1 - k^2} \quad (2.41)$$

$$\text{and } \sigma_{\theta\theta} = F'' = (1 + k)kC_2r^{k-1} - k(1 - k)C_3r^{-k-1} + 2\frac{A_1}{4 - k^2}r + \frac{A_2}{1 - k^2}$$

Finally, u can be found from the equation (2.25) as:

$$u = \beta_{12}C_2(1 + k)r^k + \beta_{12}C_3(1 - k)r^{-k} + \beta_{12}\frac{A_1}{4 - k^2}r^2 + \beta_{12}\frac{A_2}{1 - k^2}r + \beta_{22}C_2k(1 + k)r^k + \\ - \beta_{22}C_3k(1 - k)r^{-k} - 2\beta_{22}\frac{A_1}{4 - k^2}r^2 + \beta_{22}\frac{A_2}{1 - k^2}r + \alpha_{\theta\theta}Tr + \beta_{\theta\theta}cr \quad (2.42)$$

Same as the constant temperature distribution case, there are two unknown coefficients given by  $C_2$  and  $C_3$  for each layer. The equations (2.41) and (2.42) will be used as the boundary conditions to solve the problem.

### 2.3.4. Parabolic Temperature Distribution ( $T = \lambda(b^2 - r^2)$ )

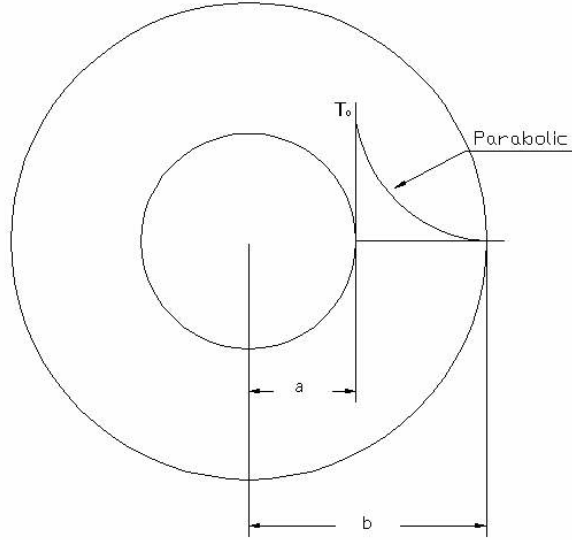


Figure 2.6 Parabolic temperature distributions on the cross-section of the tube

Temperature is equal to  $T_0$  at the inner surface where  $\lambda$  is defined as  $\lambda = \frac{T_0}{b-a}$ . If

$T$  and  $T'$  are substituted in the equation (2.30), then the equation (2.43) will be obtained

$$F''' - 2F'' + (1 - k^2)F' = \alpha_{22}(-2\lambda r)r^3 + \lambda(b^2 - r^2)\alpha_{11}r^2 + c\alpha_{33}r^2$$

$$F''' - 2F'' + (1 - k^2)F' = (\lambda\alpha_{11}b^2 + c\alpha_{33})r^2 + (-\lambda\alpha_{11} - 2\lambda\alpha_{22})r^4 \quad (2.43)$$

If  $A_1$  and  $A_2$  are defined as

$$A_1 = \lambda\alpha_{11}b^2 + c\alpha_{33}$$

$$A_2 = -\lambda\alpha_{11} - 2\lambda\alpha_{22}$$

Then the equation (2.43) becomes

$$F''' - 2F'' + (1 - k^2)F' = A_1e^{2t} + A_2e^{4t} \quad (2.44)$$

Non-homogenous solution can be written in terms of the two coefficients  $D_1$  and  $D_2$  as

$$F_{NH} = D_1e^{2t} + D_2e^{4t}$$

If  $F_{NH}$  and its derivatives are substituted in the equation (2.44), then this equation becomes

$$8.D_1e^{2t} + 64D_2.e^{4t} - 8D_1e^{2t} - 32D_2e^{4t} + (1-k^2)(2D_1e^{2t} + 4D_2e^{4t}) = A_1e^{2t} + A_2e^{4t} \quad (2.45)$$

$D_1$  and  $D_2$  can be found from the equation (2.45) as

$$A_1 = 2(1-k^2)D_1 \Rightarrow D_1 = \frac{A_1}{2(1-k^2)}$$

$$A_2 = (36-4k^2)D_2 \Rightarrow D_2 = \frac{A_2}{4(9-k^2)}$$

Then the stress function F becomes

$$F = C_1 + C_2r^{1+k} + C_3r^{(1-k)} + \frac{A_1}{2(1-k^2)}r^2 + \frac{A_2}{4(9-k^2)}r^4 \quad (2.46)$$

The stress components for parabolic temperature distribution are found as

$$\sigma_{rr} = \frac{F'}{r} = (1+k)C_2r^{k-1} + (1-k)C_3r^{-k-1} + \frac{A_1}{1-k^2} + \frac{A_2}{9-k^2}r^2 \quad (2.47)$$

$$\text{and } \sigma_{\theta\theta} = F'' = (1+k)kC_2r^{k-1} - k(1-k)C_3r^{-k-1} + \frac{A_1}{1-k^2} + 3\frac{A_2}{9-k^2}r^2$$

Thus

$$\begin{aligned} u = & \beta_{12}C_2(1+k)r^k + \beta_{12}C_3(1-k)r^{-k} + \beta_{12}\frac{A_1}{1-k^2} + \beta_{12}\frac{A_2}{9-k^2}r^3 + \beta_{22}C_2k(1+k)r^k + \\ & - \beta_{22}C_3k(1-k)r^{-k} + \beta_{22}\frac{A_1}{1-k^2}r + 3\beta_{22}\frac{A_2}{9-k^2}r^3 + \alpha_{\theta\theta}Tr + \beta_{\theta\theta}cr \end{aligned} \quad (2.48)$$

Again, for each layer, there are two unknown constants given by  $C_2$  and  $C_3$ .

#### 2.4. Example: T is constant in a plane strain problem

At this part of this study, a tube with the plane strain condition, having 4 layers will be investigated as an example. As it indicated in the previous sections, there are 2 unknown constants for each layer; therefore there are totally 8 unknown constants for a 4-layered tube.

$$\begin{bmatrix} - & - & - & - & - & - & - & - \\ - & - & - & - & - & - & - & - \\ - & - & - & - & - & - & - & - \\ - & - & - & - & - & - & - & - \\ - & - & - & - & - & - & - & - \\ - & - & - & - & - & - & - & - \\ - & - & - & - & - & - & - & - \\ - & - & - & - & - & - & - & - \end{bmatrix}_{8 \times 8} \begin{bmatrix} C_1 \\ C_2 \\ C_3 \\ C_4 \\ C_5 \\ C_6 \\ C_7 \\ C_8 \end{bmatrix}_{8 \times 1} = \begin{bmatrix} - \\ - \\ - \\ - \\ - \\ - \\ - \\ - \end{bmatrix}_{8 \times 1}$$

8 boundary conditions are required to solve this matrix. These are indicated in the Figure 2.7.

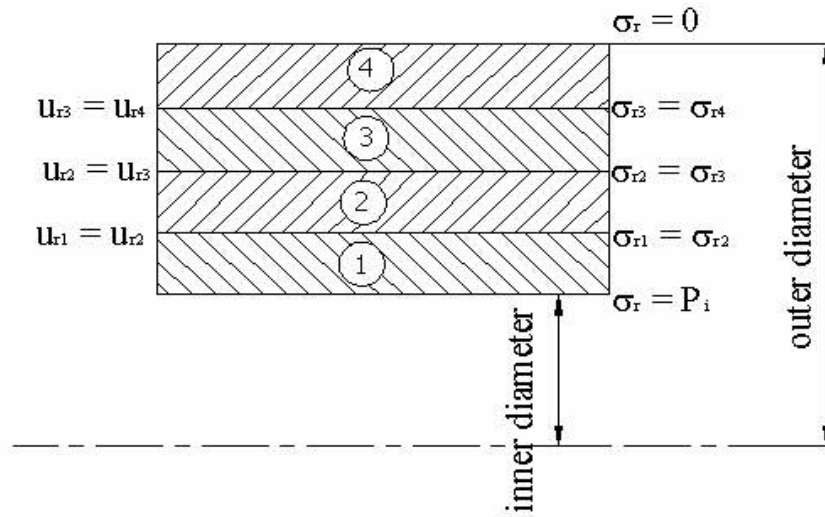


Figure 2.7 Boundary conditions of a 4-layered tube subjected to internal pressure

The equations (2.35) and (2.36) will be used to establish an 8\*8 matrix, since the boundary conditions are the equivalence of the radial stresses and radial displacements.  $\beta_{12}, \beta_{22}, \alpha_{\theta\theta}, \beta_{\theta\theta}, k$  and  $A_1$  are shown as  $\beta_{12i}, \beta_{22i}, \alpha_{\theta\theta i}, \beta_{\theta\theta i}, k_i$  and  $A_{1i}$  for  $i^{\text{th}}$  layer. Since temperature is constant for this example, it is not required to use a subscript for it.

1. Boundary Condition,  $\sigma_{rr} = P_i$  (internal pressure) where  $r_1 = a$ ,  $a$  is inner diameter

$$C_1(1+k_1)r_1^{k_1-1} + C_2(1-k_1)r_1^{-k_1-1} + \frac{A_{11}}{1-k_1^2} = P_i$$

$$\Rightarrow [(1+k_1)r_1^{k_1-1}]C_1 + [(1-k_1)r_1^{-k_1-1}]C_2 = P_i - \frac{A_{11}}{1-k_1^2}$$

2. Boundary Condition,  $\sigma_{rr1} = \sigma_{rr2}$  where  $r_2 = a + t$ ,  $t$  is the thickness of one layer

$$C_1(1+k_1)r_2^{k_1-1} + C_2(1-k_1)r_2^{-k_1-1} + \frac{A_{11}}{1-k_1^2} = C_3(1+k_2)r_2^{k_2-1} + C_4(1-k_2)r_2^{-k_2-1} + \frac{A_{12}}{1-k_2^2}$$

$$[(1+k_1)r_2^{k_1-1}]C_1 + [(1-k_1)r_2^{-k_1-1}]C_2 + [-(1+k_2)r_2^{k_2-1}]C_3 + [-(1-k_2)r_2^{-k_2-1}]C_4 =$$

$$\frac{A_{12}}{1-k_2^2} - \frac{A_{11}}{1-k_1^2}$$

3. Boundary Condition,  $u_1 = u_2$  where  $r_2 = a + t$ ,  $t$  is the thickness of one layer

$$\beta_{121}C_1(1+k_1)r_2^{k_1} + \beta_{121}C_2(1-k_1)r_2^{-k_1} + \beta_{121}\frac{A_{11}}{1-k_1^2}r_2 + \beta_{221}C_1k_1(1+k_1)r_2^{k_1} +$$

$$-\beta_{221}C_2k_1(1-k_1)r_2^{-k_1} + \beta_{221}\frac{A_{11}}{1-k_1^2}r_2 + \alpha_{\theta\theta 1}Tr_2 + \beta_{\theta\theta 1}cr_2 = \beta_{122}C_3(1+k_2)r_2^{k_2} +$$

$$\beta_{122}C_4(1-k_2)r_2^{-k_2} + \beta_{122}\frac{A_{12}}{1-k_2^2}r_2 + \beta_{222}C_3k_2(1+k_2)r_2^{k_2} - \beta_{222}C_4k_2(1-k_2)r_2^{-k_2} +$$

$$\beta_{222}\frac{A_{12}}{1-k_2^2}r_2 + \alpha_{\theta\theta 2}Tr_2 + \beta_{\theta\theta 2}cr_2$$

4. Boundary Condition,  $\sigma_{rr2} = \sigma_{rr3}$  where  $r_3 = a + 2t$ ,  $t$  is the thickness of one layer

$$C_3(1+k_2)r_3^{k_2-1} + C_4(1-k_2)r_3^{-k_2-1} + \frac{A_{12}}{1-k_2^2} = C_5(1+k_3)r_3^{k_3-1} + C_6(1-k_3)r_3^{-k_3-1} + \frac{A_{13}}{1-k_3^2}$$

$$\Rightarrow [(1+k_2)r_3^{k_2-1}]C_3 + [(1-k_2)r_3^{-k_2-1}]C_4 + [-(1+k_3)r_3^{k_3-1}]C_5 + [-(1-k_3)r_3^{-k_3-1}]C_6 =$$

$$\frac{A_{13}}{1-k_3^2} - \frac{A_{12}}{1-k_2^2}$$

5. Boundary Condition,  $u_2 = u_3$  where  $r_3 = a + 2t$ ,  $t$  is the thickness of one layer

$$\beta_{122}C_3(1+k_2)r_3^{k_2} + \beta_{122}C_4(1-k_2)r_3^{-k_2} + \beta_{122}\frac{A_{12}}{1-k_2^2}r_3 + \beta_{222}C_3k_2(1+k_2)r_3^{k_2} +$$

$$-\beta_{222}C_4k_2(1-k_2)r_3^{-k_2} + \beta_{222}\frac{A_{12}}{1-k_2^2}r_3 + \alpha_{\theta\theta 2}Tr_3 + \beta_{\theta\theta 2}cr_3 = \beta_{123}C_5(1+k_3)r_3^{k_3} +$$

$$\beta_{123}C_6(1-k_3)r_3^{-k_3} + \beta_{123}\frac{A_{13}}{1-k_3^2}r_3 + \beta_{223}C_5k_3(1+k_3)r_3^{k_3} - \beta_{223}C_6k_3(1-k_3)r_3^{-k_3} +$$

$$\beta_{223}\frac{A_{13}}{1-k_3^2}r_3 + \alpha_{\theta\theta 3}Tr_3 + \beta_{\theta\theta 3}cr_3$$

6. Boundary Condition,  $\sigma_{rr3} = \sigma_{rr4}$  where  $r_4 = a + 3t$ ,  $t$  is the thickness of one layer

$$C_5(1+k_3)r_4^{k_3-1} + C_6(1-k_3)r_4^{-k_3-1} + \frac{A_{13}}{1-k_3^2} = C_7(1+k_4)r_4^{k_4-1} + C_8(1-k_4)r_4^{-k_4-1} + \frac{A_{14}}{1-k_4^2}$$

$$\Rightarrow \left[(1+k_3)r_4^{k_3-1}\right]C_5 + \left[(1-k_3)r_4^{-k_3-1}\right]C_6 + \left[-(1+k_4)r_4^{k_4-1}\right]C_7 + \left[-(1-k_4)r_4^{-k_4-1}\right]C_8 =$$

$$\frac{A_{14}}{1-k_4^2} - \frac{A_{13}}{1-k_3^2}$$

7. Boundary Condition,  $u_3 = u_4$  where  $r_4 = a + 3t$ ,  $t$  is the thickness of one layer

$$\beta_{123}C_5(1+k_3)r_4^{k_3} + \beta_{123}C_6(1-k_3)r_4^{-k_3} + \beta_{123}\frac{A_{13}}{1-k_3^2}r_4 + \beta_{223}C_5k_3(1+k_3)r_4^{k_3} +$$

$$- \beta_{223}C_6k_3(1-k_3)r_4^{-k_3} + \beta_{223}\frac{A_{13}}{1-k_3^2}r_4 + \alpha_{\theta\theta 3}Tr_4 + \beta_{\theta\theta 3}cr_4 = \beta_{124}C_7(1+k_4)r_4^{k_4} +$$

$$\beta_{124}C_8(1-k_4)r_4^{-k_4} + \beta_{124}\frac{A_{14}}{1-k_4^2}r_4 + \beta_{224}C_7k_4(1+k_4)r_4^{k_4} - \beta_{224}C_8k_4(1-k_4)r_4^{-k_4} +$$

$$\beta_{224}\frac{A_{14}}{1-k_4^2}r_4 + \alpha_{\theta\theta 4}Tr_4 + \beta_{\theta\theta 4}cr_4$$

8. Boundary Condition,  $\sigma_{rr} = 0$  (internal pressure) where  $r_5 = b$ ,  $a$  is outer diameter

$$C_7(1+k_4)r_5^{k_4-1} + C_8(1-k_4)r_5^{-k_4-1} + \frac{A_{14}}{1-k_4^2} = 0$$

$$\Rightarrow \left[(1+k_4)r_5^{k_4-1}\right]C_7 + \left[(1-k_4)r_5^{-k_4-1}\right]C_8 = -\frac{A_{14}}{1-k_4^2}$$

## 2.5. Free-End and Pressure Vessel

Free-end case is the one where the ends of the tube are free to expand. Since there are no caps on the ends and no force acting on the tube in z-direction, the resultant force is equal to zero, which is given by

$$R = \int_{r=a}^b \sigma_{zz} 2\pi r dr = 0$$

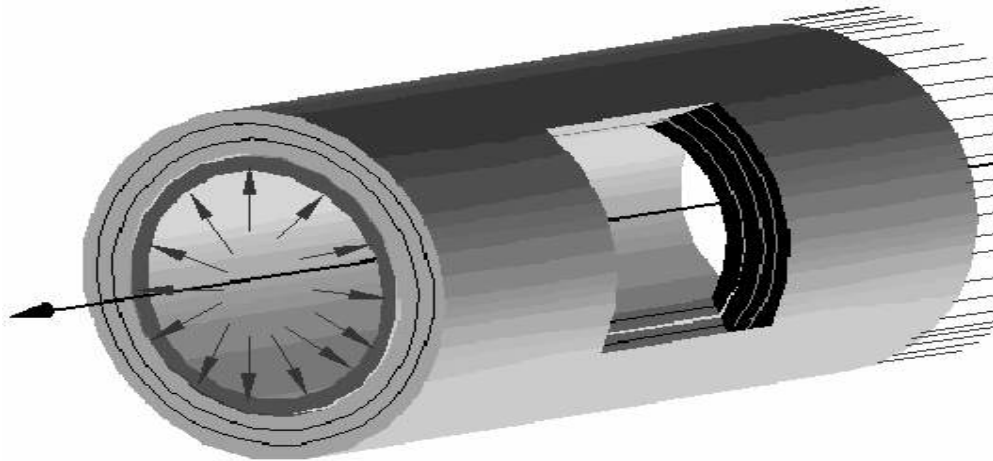


Figure 2.8 Tube with free ends to expand

On the other hand, the resultant force is not equal to zero for pressure vessel. Since two caps at the ends close the tube, the resultant force in z-direction is equal to the force created by internal pressure on the caps, which is given by

$$R = \int_{r=a}^b \sigma_{zz} 2\pi r dr = \pi a^2 P_i$$

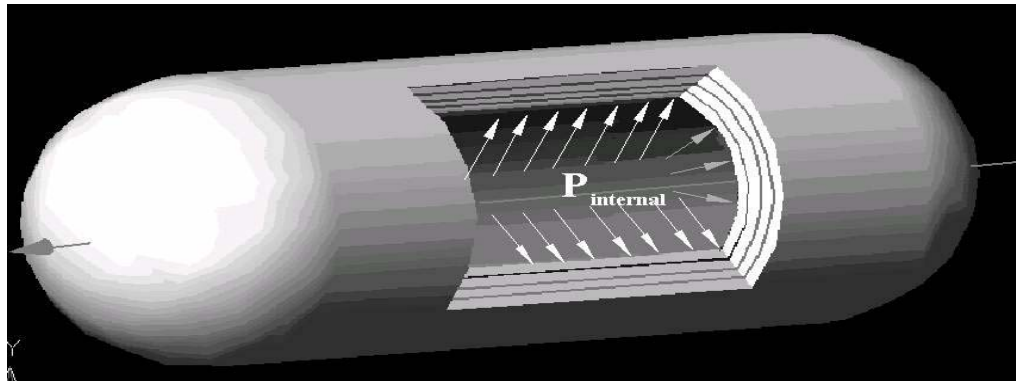


Figure 2.9 Pressure vessel subjected to internal pressure

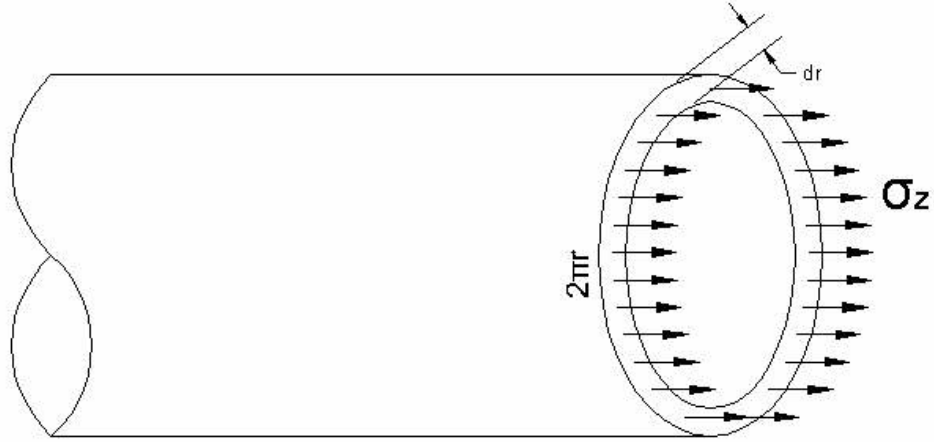


Figure 2.10 Cross section of a pressure vessel

For both cases, a parameter D can be defined as

$$\varepsilon_{zz} = a_{13}\sigma_{rr} + a_{32}\sigma_{\theta\theta} + a_{33}\sigma_{zz} + \alpha_z T + \beta_z c = D \quad (2.49)$$

Then, from the equation (2.49),  $\sigma_{zz}$  can be found as

$$\sigma_{zz} = \frac{D}{a_{33}} - \left( \frac{a_{13}}{a_{33}}\sigma_{rr} - \frac{a_{23}}{a_{33}}\sigma_{\theta\theta} - \frac{\alpha_z}{a_{33}}T - \frac{\beta_z}{a_{33}}c \right) \quad (2.50)$$

If  $\sigma_{zz}$  is substituted in the equations (2.15) and (2.16), then the following two equations will be obtained

$$\begin{aligned} \varepsilon_{rr} = \frac{du}{dr} = & a_{11}\sigma_{rr} + a_{12}\sigma_{\theta\theta} + \frac{a_{13}}{a_{33}}D - \frac{a_{13}^2}{a_{33}}\sigma_{rr} - \frac{a_{13}a_{23}}{a_{33}}\sigma_{\theta\theta} - \frac{a_{13}}{a_{33}}\alpha_z T - \frac{a_{13}}{a_{33}}\beta_z c + \\ & + \alpha_r T + \beta_r c \end{aligned} \quad (2.51)$$

$$\begin{aligned} \varepsilon_{\theta\theta} = \frac{u}{r} = & a_{12}\sigma_{rr} + a_{22}\sigma_{\theta\theta} + \frac{a_{23}}{a_{33}}D - \frac{a_{23}a_{13}}{a_{33}}\sigma_{rr} - \frac{a_{23}^2}{a_{33}}\sigma_{\theta\theta} - \frac{a_{23}}{a_{33}}\alpha_z T - \frac{a_{23}}{a_{33}}\beta_z c + \\ & + \alpha_\theta T + \beta_\theta c \end{aligned} \quad (2.52)$$

or these two equations (2.51) and (2.52) can be written simply as

$$\varepsilon_{rr} = \frac{du}{dr} = \beta_{11}\sigma_{rr} + \beta_{12}\sigma_{\theta\theta} + \alpha_{rr}T + \beta_{rr}c + \beta_{13}D \quad (2.53)$$

$$\varepsilon_{\theta\theta} = \frac{u}{r} = \beta_{12}\sigma_{rr} + \beta_{22}\sigma_{\theta\theta} + \alpha_{\theta\theta}T + \beta_{\theta\theta}c + \beta_{23}D \quad (2.54)$$

where  $\beta_{11}$ ,  $\beta_{12}$ ,  $\beta_{22}$ ,  $\alpha_{rr}$ ,  $\alpha_{\theta\theta}$ ,  $\beta_{rr}$  and  $\beta_{\theta\theta}$  are defined in the equations (2.21) and  $\beta_{13}$  and  $\beta_{23}$  are defined as

$$\beta_{13} = \frac{a_{13}}{a_{33}}$$

$$\beta_{23} = \frac{a_{23}}{a_{33}}$$

If the derivative of u is taken with respect to r in the equation (2.54), then this will be equal to  $\varepsilon_{rr}$  in the equation (2.53). Substituting  $\sigma_{rr} = \frac{F'}{r}$  and  $\sigma_{\theta\theta} = F''$  in the equation as well, it becomes

$$\begin{aligned} \beta_{11} \frac{F'}{r} + \beta_{12} F'' + \alpha_{rr} T + \beta_{rr} c + \beta_{13} D &= \frac{d}{dr} \left[ \beta_{12} \frac{F'}{r} r + \beta_{22} F'' r + \alpha_{\theta\theta} T r + \beta_{\theta\theta} c r \right] + \\ &+ \frac{d}{dr} (\beta_{23} D r) \text{ or} \\ r^3 \beta_{22} F''' + r^2 \beta_{22} F'' - r \beta_{11} F' &= (\alpha_{rr} - \alpha_{\theta\theta}) T r^2 + (\beta_{rr} - \beta_{\theta\theta}) c r^2 - \alpha_{\theta\theta} \frac{dT}{dr} r^3 + \\ &+ (\beta_{13} - \beta_{23}) D r^2 \text{ or} \\ r^3 F''' + r^2 F'' - k^2 r F' &= \frac{(\alpha_{rr} - \alpha_{\theta\theta})}{\beta_{22}} T r^2 + \frac{(\beta_{rr} - \beta_{\theta\theta})}{\beta_{22}} c r^2 - \frac{\alpha_{\theta\theta}}{\beta_{22}} \frac{dT}{dr} r^3 + \frac{(\beta_{13} - \beta_{23})}{\beta_{22}} D r^2 \end{aligned} \quad (2.55)$$

where k is defined as  $k = \sqrt{\frac{\beta_{11}}{\beta_{22}}}$

If  $\alpha_a$ ,  $\beta_a$ ,  $\alpha_b$  and  $\beta_d$  are defined as

$$\alpha_a = \frac{(\alpha_{rr} - \alpha_{\theta\theta})}{\beta_{22}}$$

$$\beta_a = \frac{(\beta_{rr} - \beta_{\theta\theta})}{\beta_{22}}$$

$$\alpha_b = \frac{\alpha_{\theta\theta}}{\beta_{22}}$$

$$\beta_d = \frac{(\beta_{13} - \beta_{23})}{\beta_{22}}$$

Then, the equation (2.55) becomes

$$r^3 F''' + r^2 F'' - k^2 r F' = T \alpha_a e^{2t} + c \beta_a e^{2t} - \alpha_b T' e^{3t} + D \beta_d e^{2t} \quad (2.56)$$

To find the homogenous solution, it is required to define  $r$  and  $F$  as

$$r = e^t$$

$$\frac{dF}{dr} = \frac{dF}{dt} \frac{dt}{dr} = e^{-t} F'$$

Putting  $F$  and its derivatives into the equation (2.56), then the homogenous solution can be found as

$$(e^t)^3 (3e^{-3t} F' - 3e^t F'' + e^{-3t} F''') + (e^t)^2 (-e^{-2t} F' + e^{-2t} F'') - k^2 r (e^{-t} F') = 0$$

$$\text{or } F''' - 2F'' + (1 - k^2)F' = 0$$

The roots of the homogenous solution are  $R_1 = 0$ ,  $R_2 = 1 + k$  and  $R_3 = 1 - k$

Therefore, the homogenous solution is presented as

$$F_h = C_1 + C_2 e^{(1+k)t} + C_3 e^{(1-k)t} \text{ or}$$

$$F_h = C_1 + C_2 r^{(1+k)} + C_3 r^{(1-k)}$$

### 2.5.1. Non-homogenous Solution

If the roots of the homogenous solution are put into the equation (2.56), then this equation becomes

$$F''' - 2F'' + (1 - k^2)F' = T\alpha_a e^{2t} + c\beta_a e^{2t} - \alpha_b T' e^{3t} + D\beta_d e^{2t} \quad (2.57)$$

### 2.5.2. Constant Temperature Distribution ( $T = T_0$ )

If Temperature and its derivative are substituted in the equation (2.57), it becomes

$$F''' - 2F'' + (1 - k^2)F' = T_0\alpha_a e^{2t} + c\beta_a e^{2t} + D\beta_d e^{2t} \quad (2.58)$$

To solve the equation (2.58), it is required to define the a non-homogenous function by a coefficient as

$$F_{NH} = A.e^{2t}$$

Putting the function  $F_{NH}$  into the equation (2.58), then this equation becomes

$$8Ae^{2t} - 2(4A.e^{2t}) + (1 - k^2)2A.e^{2t} = T_0\alpha_a e^{2t} + c\beta_a e^{2t} + D\beta_d e^{2t} \quad (2.59)$$

Then from the equation (2.59), the coefficient  $A$  can be found as

$$A = \frac{T_0\alpha_a + c\beta_a + D\beta_d}{2(1 - k^2)}$$

Thus

$$F = C_1 + C_2 r^{1+k} + C_3 r^{1-k} + Ar^2$$

Then  $\sigma_{rr}$  and  $\sigma_{\theta\theta}$  are found as

$$\sigma_{rr} = \frac{F'}{r} = (1+k)C_1 r^{k-1} + (1-k)C_2 r^{-k-1} + 2A \quad (2.60)$$

$$\sigma_{\theta\theta} = F'' = (1+k)kC_1 r^{k-1} - k(1-k)C_2 r^{-k-1} + 2A$$

and the radial displacement can be written as

$$u = \beta_{12}(1+k)C_1 r^k + \beta_{12}(1-k)C_2 r^{-k} + 2\beta_{12}Ar + \beta_{22}(1+k)kC_1 r^k - \beta_{22}k(1-k)C_2 r^{-k} + 2\beta_{22}Ar + \alpha_{\theta\theta}Tr + \beta_{\theta\theta}cr + \beta_{23}Dr \quad (2.61)$$

There are two unknown constants for each layer as  $C_1$  and  $C_2$ . In addition to these constants, there is one more unknown, D for the whole structure, which will be used to make iteration in the numerical program.

### 2.5.3. Linear Temperature Distribution ( $T = \lambda(b-r)$ )

Temperature is equal to  $T_0$  at the inner surface where  $\lambda$  is defined as  $\lambda = \frac{T_0}{b-a}$ .

The derivative of T is equal to  $-\lambda$ .

$$T' = -\lambda$$

Then the non-homogenous equation becomes

$$F''' - 2F'' + (1-k^2)F' = \lambda(b-r)\alpha_a e^{2t} + c\beta_a e^{2t} + \lambda\alpha_b e^{3t} + D\beta_d e^{2t} \text{ or}$$

$$F''' - 2F'' + (1-k^2)F' = (\lambda b\alpha_a + c\beta_a + D\beta_d)e^{2t} + (-\lambda\alpha_a + \lambda\alpha_b)e^{3t} \quad (2.62)$$

Defining  $A_1$  and  $A_2$  as

$$A_1 = \lambda b\alpha_a + c\beta_a + D\beta_d$$

$$A_2 = -\lambda\alpha_a + \lambda\alpha_b$$

Then the equation (2.62) can be written as

$$F''' - 2F'' + (1-k^2)F' = A_1 e^{2t} + A_2 e^{3t} \quad (2.63)$$

To find the non-homogenous solution, it is required to define the function F in terms of two coefficients as  $B_1$  and  $B_2$ .

$$F_{NH} = B_1 e^{2t} + B_2 e^{3t}$$

If  $F_{NH}$  is substituted in the equation (2.63), then this equation becomes

$$8B_1e^{2t} + 27B_2e^{3t} - 2(4B_1e^{2t} + 9B_2e^{3t}) + (1-k^2)(2B_1e^{2t} + 3B_2e^{3t}) = A_1e^{2t} + A_2e^{3t} \quad (2.64)$$

$B_1$  and  $B_2$  can be found from the equation (2.64) as

$$B_1(8-8+2-2k^2) = A_1 \Rightarrow B_1 = \frac{A_1}{2(1-k^2)}$$

$$B_2(27-18+3-3k^2) = A_2 \Rightarrow B_2 = \frac{A_2}{3(4-k^2)}$$

Thus

$$F = C_1 + C_2r^{(1+k)} + C_3r^{(1-k)} + \frac{A_1}{2(1-k^2)}r^2 + \frac{A_2}{3(4-k^2)}r^3$$

Then the stress components  $\sigma_{rr}$  and  $\sigma_{\theta\theta}$  are found as

$$\sigma_{rr} = \frac{F'}{r} = (1+k)C_2r^{k-1} + (1-k)C_3r^{-k-1} + \frac{A_1}{1-k^2} + \frac{A_2}{4-k^2}r \quad (2.65)$$

$$\sigma_{\theta\theta} = F'' = (1+k)kC_2r^{k-1} - k(1-k)C_3r^{-k-1} + \frac{A_1}{1-k^2} + 2\frac{A_2}{4-k^2}r$$

Finally, the radial displacement can be written as

$$u = \beta_{12}(1+k)C_2r^k + \beta_{12}(1-k)C_3r^{-k} + \beta_{12}\frac{A_1}{1-k^2}r + \beta_{12}\frac{A_2}{4-k^2}r^2 + \beta_{22}(1+k)kC_2r^k - \beta_{22}k(1-k)C_3r^{-k} + \beta_{22}\frac{A_1}{1-k^2}r + 2\beta_{22}\frac{A_2}{4-k^2}r^2 + \alpha_{\theta\theta}Tr + \beta_{\theta\theta}cr + \beta_{23}Dr \quad (2.66)$$

Again there are two unknown constants given by  $C_2$  and  $C_3$  for each layer with linear temperature distribution, in addition to D.

#### 2.5.4. Parabolic Temperature Distribution ( $T = \lambda(b^2 - r^2)$ )

Temperature is equal to  $T_0$  at the inner surface where  $\lambda$  is defined as  $\lambda = \frac{T_0}{b-a}$ .

Thus

$$T' = -2\lambda r$$

Putting  $T$  and  $T'$  into the equation (2.57), then the equation becomes

$$F''' - 2F'' + (1-k^2)F' = \lambda(b^2 - r^2)\alpha_a e^{2t} + c\beta_a e^{2t} + 2\lambda r\alpha_b e^{3t} + D\beta_d e^{2t} \text{ or}$$

$$F''' - 2F'' + (1-k^2)F' = (\lambda b^2\alpha_a + c\beta_a + D\beta_d)e^{2t} + (-\lambda\alpha_a + 2\lambda\alpha_b)e^{4t} \quad (2.67)$$

If  $A_1$  and  $A_2$  are defined as

$$A_1 = \lambda b^2 \alpha_a + c \beta_a + D \beta_d$$

$$A_2 = -\lambda \alpha_a + 2\lambda \alpha_b$$

Then the equation (2.67) becomes

$$F''' - 2F'' + (1 - k^2)F' = A_1 e^{2t} + A_2 e^{4t} \quad (2.68)$$

Non-homogenous solution can be defined as in terms of two coefficients as

$$F_{NH} = B_1 e^{2t} + B_2 e^{4t}$$

Putting  $F_{NH}$  and its derivatives into the equation (2.68), then this equation becomes

$$8B_1 e^{2t} + 64B_2 e^{4t} - 8B_1 e^{2t} - 32B_2 e^{4t} + (1 - k^2)(2B_1 e^{2t} + 4B_2 e^{4t}) = A_1 e^{2t} + A_2 e^{4t} \quad (2.69)$$

$B_1$  and  $B_2$  can be found from the equation (2.69) as

$$B_1(8 - 8 + 2 - 2k^2) = A_1 \Rightarrow B_1 = \frac{A_1}{2(1 - k^2)}$$

$$B_2(64 - 32 + 4 - 4k^2) = A_2 \Rightarrow B_2 = \frac{A_2}{4(9 - k^2)}$$

Then the stress function can be written as

$$F = C_1 + C_2 r^{(1+k)} + C_3 r^{(1-k)} + \frac{A_1}{2(1 - k^2)} r^2 + \frac{A_2}{4(9 - k^2)} r^4$$

$\sigma_{rr}$  and  $\sigma_{\theta\theta}$  for parabolic temperature distribution can be found as

$$\Rightarrow \sigma_{rr} = \frac{F'}{r} = (1 + k)C_2 r^{k-1} + (1 - k)C_3 r^{-k-1} + \frac{A_1}{1 - k^2} + \frac{A_2}{9 - k^2} r^2 \quad (2.70)$$

$$\text{and } \sigma_{\theta\theta} = F'' = (1 + k)kC_2 r^{k-1} - k(1 - k)C_3 r^{-k-1} + \frac{A_1}{1 - k^2} + 3\frac{A_2}{9 - k^2} r^2$$

And radial displacement is found as

$$u = \beta_{12}(1 + k)C_2 r^k + \beta_{12}(1 - k)C_3 r^{-k} + \beta_{12} \frac{A_1}{1 - k^2} r + \beta_{12} \frac{A_2}{9 - k^2} r^3 + \beta_{22}(1 + k)kC_2 r^k \\ - \beta_{22}k(1 - k)C_3 r^{-k} + \beta_{22} \frac{A_1}{1 - k^2} r + 3\beta_{22} \frac{A_2}{9 - k^2} r^3 + \alpha_{\theta\theta} \lambda (b^2 - r^2) r + \beta_{\theta\theta} c r + \beta_{23} D r \quad (2.71)$$

Again there are two unknown constants for each layer, in addition to D. The equations (2.70) and (2.71) will be used as boundary conditions to solve the problem.

## 2.6. Hoffman Failure Criteria

Failure prediction for a laminate requires knowledge of the stresses or strains or sometimes both in each lamina. In the previous sections of this study, the stresses under hygrothermal loading acting in the principal directions for each lamina have been found. To select a proper failure criteria, it is required to know the advantages and disadvantages of each failure criteria and the material properties as well. In case that compressive and tensile strength of a structure are different which is the case of the selected structure, Hoffmann criteria and Tsai-Wu give better and consistent solution than Tsai-Hill, since Tsai-Hill, which is an extension of von Mises' yield criterion, is useful for anisotropic materials those have the same yield points in tension and compression. For this problem, Hoffman failure criteria is selected for failure check, since it is more practical to use than Tsai-Wu. The advantages of Hoffman criteria are as listed below:

1. In design , the Hoffman criteria is the simplest criterion of all the criteria
2. Interaction between failure modes is treated instead of separate criteria for failure like the maximum stress or maximum strain failure criteria.
3. A single failure criterion is used in all quadrants because of different strengths in tension and compression.

Tsai-Wu criteria has the following advantages:

1. Increased curve fitting capability over the Tsai-Hill and Hoffman criteria because of an additional term in the equation.
2. The additional term can be determined only with an expensive and difficult biaxial test.

Therefore the use of Hoffman criterion is easier than Tsai -Wu criterion.

To account for different strengths in tension and compression, Hoffman added linear terms to Hill's equation. (The basis for the Tsai-Hill criteria) [3]. The summation of the stresses with linear terms is equal to an index, which is defined as Hoffman index and shown as H, which is given by

$$K_1.(\sigma_2 - \sigma_3)^2 + K_2.(\sigma_3 - \sigma_1)^2 + K_3.(\sigma_1 - \sigma_2)^2 + K_4.\sigma_1 + K_5.\sigma_2 + K_6.\sigma_3 + K_7.\tau_{23}^2 + K_8.\tau_{31}^2 + K_9.\tau_{12}^2 = H \quad (2.72)$$

If the Hoffman index exceeds 1, the structure will fail.

The material, which was used in the computer-program, is Epoxy-Carbon [6] laminate (T300/N5208). The mechanical properties of the material are presented as

$X_T$  : Ultimate tensile strength in fiber direction (MPA): 1500

$X_C$  : Ultimate compressive strength in fiber direction (MPA): 1500

$Y_T$  : Ultimate tensile strength in matrix direction (MPA): 40

$Y_C$  : Ultimate compressive strength in matrix direction (MPA): 146

$Z_T = Y_T$  and  $Z_C = Y_C$  Ultimate compressive and tensile strengths in z-direction are assumed to be equal in y-direction

S: Ultimate in-plane shears strength (MPA): 68 (assumed to be equal for all directions)

$\alpha_1$ : Thermal expansion coefficient in fiber direction ( $10^{-6}/C^{\circ}$ ): 0.02

$\alpha_2$ : Thermal expansion coefficient in matrix direction ( $10^{-6}/C^{\circ}$ ): 22.5

Since matrix is made of epoxy and fiber is carbon, thermal expansion in matrix direction is much more greater than in fiber direction.

$\beta_1$ : Moisture expansion coefficient in fiber direction: 0

$\beta_2$ : Moisture expansion coefficient in matrix direction: 0.6

where the coefficients  $K_i$  are determined from the 9 strengths in principal coordinates:  $X_t, X_c, Y_t, Y_c, Z_t, Z_c, S_{23}, S_{31}$  and  $S_{12}$ .

For this problem, there are no shear stresses, hence  $K_7 = K_8 = K_9 = 0$

Therefore the equation (2.72) reduces to

$$K_1.(\sigma_2 - \sigma_3)^2 + K_2.(\sigma_3 - \sigma_1)^2 + K_3.(\sigma_1 - \sigma_2)^2 + K_4.\sigma_1 + K_5.\sigma_2 + K_6.\sigma_3 = 1 \quad (2.73)$$

The coefficients are determined by applying normal stress in several directions.

1) Apply only tensile stress in fiber direction

$$\sigma_1 = X_t$$

$$\sigma_2 = \sigma_3 = 0$$

Put into the equation (2.73)

$$K_2(-\sigma_1)^2 + K_3\sigma_1^2 + K_4\sigma_1 = 1$$

$$K_2 X_t^2 + K_3 X_t^2 + K_4 X_t = 1 \quad (2.74)$$

2) Apply only compressive stress in fiber direction

$\sigma_1 = -X_c$  (For compressive stresses, use  $(-X_c)$ , since  $X_c$  is an inherently negative number for Hoffman criteria [3].

$$\sigma_2 = \sigma_3 = 0$$

Put into the equation (2.73)

$$K_2 (-\sigma_1)^2 + K_3 \sigma_1^2 + K_4 \sigma_1 = 1$$

$$K_2 X_c^2 + K_3 X_c^2 - K_4 X_c = 1 \quad (2.75)$$

Since  $X_t = X_c$  from the equations (2.74) and (2.75),  $K_4$  can be easily found as

$$K_4 = 0$$

$$\text{And } K_2 + K_3 = \frac{1}{X_t^2} \quad (2.76)$$

3) Apply only tensile stress in (2) matrix direction

$$\sigma_2 = Y_t$$

$$\sigma_1 = \sigma_3 = 0$$

Putting these into the equation (2.73), then the equation (2.77) will be obtained as

$$K_1 Y_t^2 + K_3 Y_t^2 + K_5 Y_t = 1 \quad (2.77)$$

4) Apply only compressive stress in (2) matrix direction

$$\sigma_2 = -Y_c$$

$$\sigma_1 = \sigma_3 = 0$$

If these equations are put into equation (2.73), then the following equation is obtained

$$K_1 (-Y_c)^2 + K_3 (-Y_c)^2 + K_5 (-Y_c) = 1$$

$$K_1 Y_c^2 + K_3 Y_c^2 - K_5 Y_c = 1 \quad (2.78)$$

**5) Apply only tensile stress in (3) matrix direction**

Since the structure behaves similarly in (2) and (3) directions, it can be written that

$$\sigma_3 = Y_t$$

$$\sigma_1 = \sigma_2 = 0$$

If these equations are put into equation (2.73), then we obtain

$$K_1 Y_t^2 + K_2 Y_t^2 + K_6 Y_t = 1 \quad (2.79)$$

**6) Apply only compressive stress in (3) matrix direction**

$$\sigma_3 = -Y_c$$

$$\sigma_1 = \sigma_2 = 0$$

Putting these equations into the equation (2.73), then the following equation is obtained as

$$K_1 (-Y_c)^2 + K_2 (-Y_c)^2 + K_6 (-Y_c) = 1$$

$$K_1 Y_c^2 + K_2 Y_c^2 - K_6 Y_c = 1 \quad (2.80)$$

From the equations (2.68) to (2.71), the coefficients are determined as

$$K_6 = K_5 = 181576 * 10^{-7} \frac{1}{MPA^2}$$

$$K_3 = K_2 = 2 * 10^{-7} \frac{1}{MPA^2}$$

$$K_1 = 1710 * 10^{-7} \frac{1}{MPA^2}$$

Then the Hoffman equation becomes

$$1710.10^{-7} (\sigma_2 - \sigma_3)^2 + 2.10^{-7} (\sigma_3 - \sigma_1)^2 + 2.10^{-7} (\sigma_1 - \sigma_2)^2 + 181576.10^{-7} \sigma_2 + 181576.10^{-7} \sigma_3 = 1$$

This relation is used for the failure check of the cylinders.

## CHAPTER 3

### NUMERICAL RESULTS AND DISCUSSIONS

In this chapter, the numerical results of the computer program are tabulated and some outputs of these results are discussed. In these solutions, the computer program has been run for four layers oriented as [30/-30/-30/30], [45/-45/-45/45] and [60/-60/-60/60] under different hygrothermal and mechanical conditions. The selected material is Epoxy-Carbon laminate (T300/N5208). The material properties are presented in the chapter 2, section 2.6. It is assumed that the material starts to degrade at 150° C, so the program is stopped to run at this temperature rate. The stresses calculated for the interface surfaces and boundary surfaces are presented in the tables for 5 surfaces for each loading case. The Hoffman index are calculated for each of 5 surfaces, but the indexes given in this chapter are the highest index between them, since it is the worst situation which may cause failure of the structure. Sometimes, it is preferred also to make a deeper analysis by calculating the stresses on the matrix plane, which is the weakest plane and may cause failure of the structure since it has lower strength values. The projection of the calculated stresses on the matrix plane can be found as

$$\sigma_m = \sigma_{zz} \cdot \sin^2(-\alpha) + \sigma_{\theta\theta} \cdot \cos^2(-\alpha) \quad (3.1)$$

since  $+\alpha$  is the fiber plane,  $\sigma_m$  is calculated for  $-\alpha$ .

#### 3.1 Plane Strain

The results for plane strain case are summarized in the following graphs:

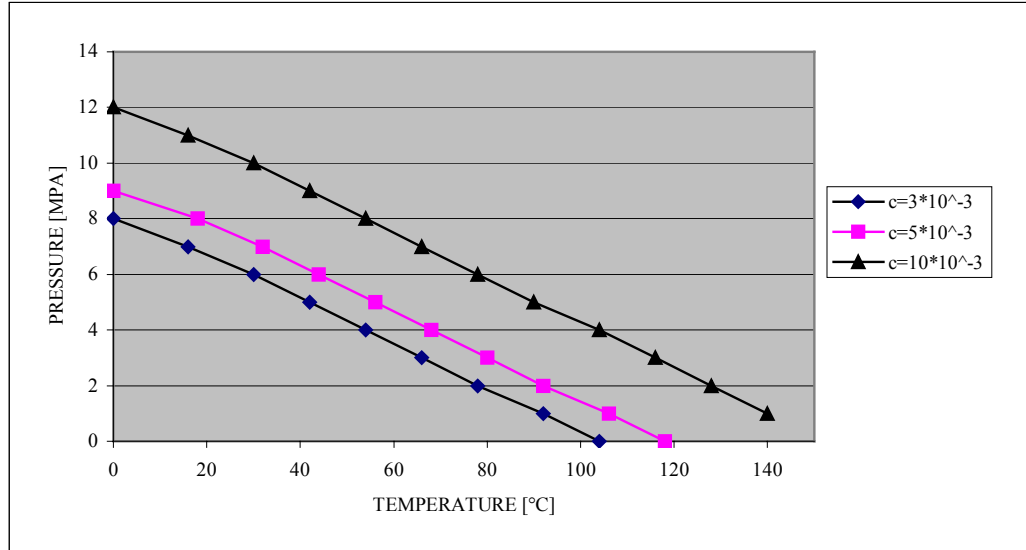


Figure 3.1. Fail pressure of a vessel with [45°/-45°] for parabolic temperature distribution

For parabolic temperature distribution, with increasing pressure rate, failure temperature decreases, since the stresses inside and outside of the tube have different sign for parabolic temperature distribution, the value of stresses increases.  $\sigma_{zz}$  is tensile at low temperatures, but then with increasing temperature it will be compressive around the inner surface, and tensile around the outer surface due to temperature distribution, since the temperature value is the highest at the inner surface and it is equal to  $T_0$ . At the outer surface, the effects of both temperature and pressure can be noticed.  $\sigma_{zz}$  is going to be compressive with increasing temperature since the effect of temperature is greater than the effect of internal pressure which is in opposite sign of the temperature effect where high temperature results compressive stress due to plane strain conditions in which the tube is prevented to expand..

$\sigma_{rr}$  is always compressive due to plane strain conditions where  $\sigma_{\theta\theta}$  is always tensile due to internal pressure. . The magnitude of  $\sigma_{rr}$  is the highest at the inner surface and 0 at the outer surface due to boundary conditions. Failure occurs mostly at the outer surface where both  $\sigma_{\theta\theta}$  and  $\sigma_{zz}$  are tensile. The Hoffman index is calculated smaller than 1 as  $4.313 \cdot 10^{-3}$  for a 45° layered tube for parabolic temperature distribution and  $c=3 \cdot 10^{-3}$  with the temperature value of 0°C and

internal pressure of 5MPa, therefore for this condition failure does not occur where  $\sigma_{\theta\theta}$  and  $\sigma_{zz}$  are tensile, whereas  $\sigma_{rr}$  is compressive.  $\sigma_m$  is calculated as 19.99MPa. The stresses are tabulated in Table 3.1.

Table 3.1. The stress distribution at P=5MPa, T=0°C

Surface	D	$\sigma_{rr}$	$\sigma_{\theta\theta}$	$\sigma_{zz}$
1	30	-5,00	39,91	6,85
2	31	-3,58	38,46	5,89
3	32	-2,28	37,32	5,15
4	33	-1,09	36,45	4,59
5	34	0	35,8	4,19

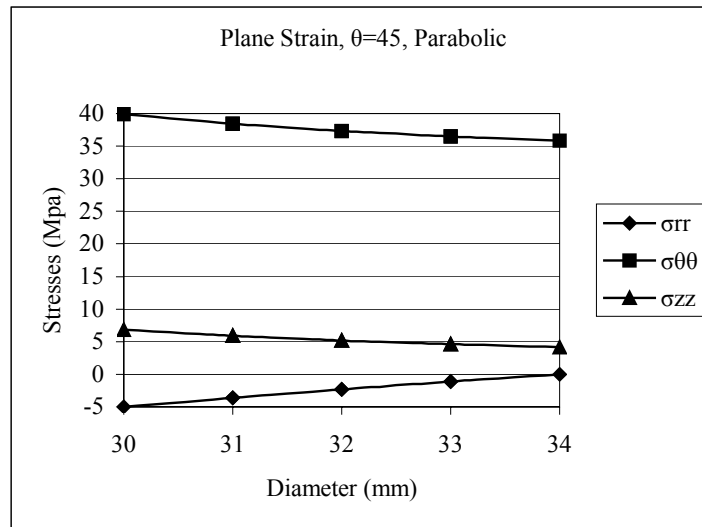


Figure 3.2. The stress distribution at P=5MPa, T=0°C

If T reaches to 42° C for P=5MPa, failure occurs since the Hoffman index is calculated as 1.0207. The stresses are tabulated in Table 3.2.

Table 3.2. The stress distribution at P=5MPa, T=42°C

Surface	D	$\sigma_{rr}$	$\sigma_{\theta\theta}$	$\sigma_{zz}$
1	30	-5,00	16,07	-22,89
2	31	-4,15	26,65	-12,08
3	32	-3,02	37,37	-1,04
4	33	-1,63	48,29	10,26
5	34	0	59,45	21,86

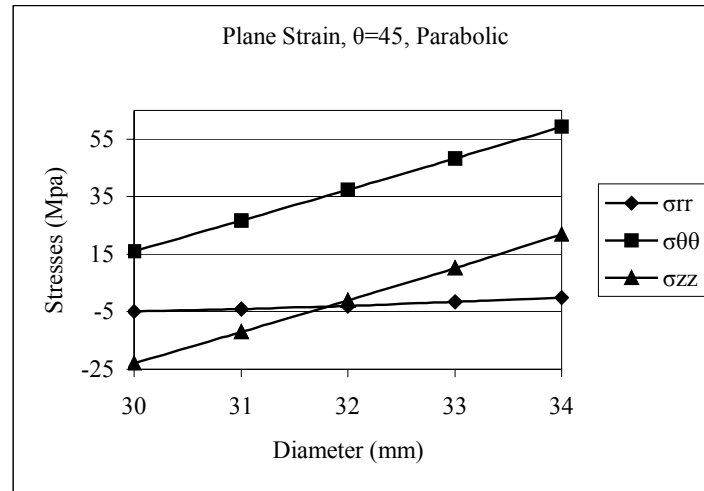


Figure 3.3. The stress distribution at P=5MPa, T=42°C

The tube with 45° layered fibers and parabolic temperature distribution, where internal pressure is 8MPa, fails at the temperature value of 0°C due to the internal pressure at the inner surface.

$$\sigma_m = 64.51 * \cos^2(-45) + 24.99 * \sin^2(-45) = 44.75MPa$$

The stress components in matrix direction is greater than the strength, hence at internal pressure rate of 8 MPa, the tube fails at 0° C. The stress distributions are tabulated in Table 3.3.

Table 3.3. The stress distribution at P=8MPa, T=0°C for moisture concentration of  $3 \cdot 10^{-3}$

Surface	D	$\sigma_{rr}$	$\sigma_{\theta\theta}$	$\sigma_{zz}$
1	30	-8,00	64,51	24,99
2	31	-5,71	61,85	23,19
3	32	-3,63	59,71	21,75
4	33	-1,74	58,00	20,63
5	34	0	56,67	19,78

The Hoffman index is calculated as 1.1434.

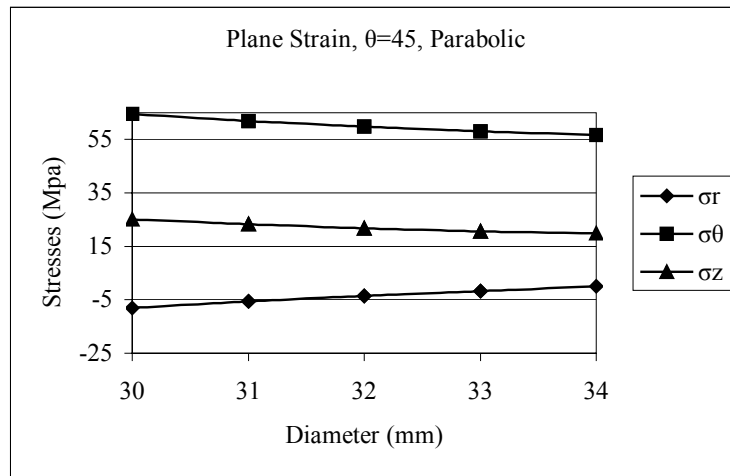


Figure 3.4. The stress distribution at P=8MPa, T=0°C for moisture concentration of  $3 \cdot 10^{-3}$

Before this study, it was expected that with increasing moisture concentration, the tube would fail at the lower internal pressure values. But as it can be seen from the results, with the increasing moisture concentration, the fail pressure is also increasing, since in this study, there are several factors that affect failure of the tubes. Sometimes, these effects may act reverse. The stress components of  $\sigma_{zz}$  is superposition of the hygrothermal and internal pressure effects where  $\sigma_{zz} = \nu \cdot (\sigma_{rr} + \sigma_{\theta\theta})$ . The parts of  $\sigma_{zz}$  created by internal pressure is tensile, the other part of  $\sigma_{zz}$  created by hygrothermal loading is compressive due to plane strain conditions.

At the temperature value of 0°C and internal pressure of 8MPa, the stress distribution of a tube with 45° layered fibers with parabolic temperature distribution for 3 different moisture concentrations are tabulated in Tables 3.3-5.

Table 3.4. The stress distribution for moisture concentration of  $5*10^{-3}$

Surface	D	$\sigma_{rr}$	$\sigma_{\theta\theta}$	$\sigma_{zz}$
1	30	-8	63,78	9,4
2	31	-5,72	61,5	7,89
3	32	-3,65	59,72	6,73
4	33	-1,75	58,36	5,87
5	34	0	57,35	5,26

The Hoffman index is calculated as  $7.3585*10^{-1}$ .

Table 3.5. The stress distribution for moisture concentration of  $10*10^{-3}$

Surface	D	$\sigma_{rr}$	$\sigma_{\theta\theta}$	$\sigma_{zz}$
1	30	-8	61,93	-29,55
2	31	-5,77	60,63	-30,34
4	32	-3,71	59,76	-30,82
7	33	-1,79	59,25	-31,05
8	34	0	59,04	-31,05

The Hoffman index is calculated as  $2.875*10^{-1}$ .

As it can be seen from Tables 3.3-5,  $\sigma_{zz}$  values are going to be negative for  $c=10*10^{-3}$ , since hygrothermal loading results in an increase of  $\sigma_{zz}$  value as negative. So, superposition of  $\sigma_{zz}$  gives smaller tensile stress or compressive stress for  $c=10*10^{-3}$ . Therefore, the tube fails later for  $c=10*10^{-3}$  than  $c=3*10^{-3}$  where the tube for moisture concentration of  $3*10^{-3}$  fails at 0° C for the internal pressure value of 8MPa, since stress component in matrix direction is found greater than the strength in this direction.

$$c=3*10^{-3} \Rightarrow \sigma_m = 24.99 * \cos^2(-45) + 64.51 * \sin^2(-45) = 44.75MPa$$

$$c=5*10^{-3} \Rightarrow \sigma_m = 9.4 * \cos^2(-45) + 63.78 * \sin^2(-45) = 36.59MPA$$

$$c=10*10^{-3} \Rightarrow \sigma_m = -29.55 * \cos^2(-45) + 61.93 * \sin^2(-45) = 16.19MPA$$

In order to see the moisture effect, fail temperatures of a tube with 45° layered fibers for parabolic temperature distribution and for different moisture concentration values are investigated and tabulated in Table 3.6 for the absence of internal pressure.

Table 3.6.Fail temperatures for various moisture concentrations

c	3*10 <sup>-3</sup>	5*10 <sup>-3</sup>	10*10 <sup>-3</sup>	15*10 <sup>-3</sup>	20*10 <sup>-3</sup>	30*10 <sup>-3</sup>	35*10 <sup>-3</sup>	40*10 <sup>-3</sup>
T <sub>fail</sub>	104	118	152	134	102	38	6	0

As it can be followed from Table 3.6, the effect of moisture can be easily realized for high moisture concentration. But as it is explained previously, for small moisture concentration values, moisture effect may act reverse and the tube may fail at higher temperature values.

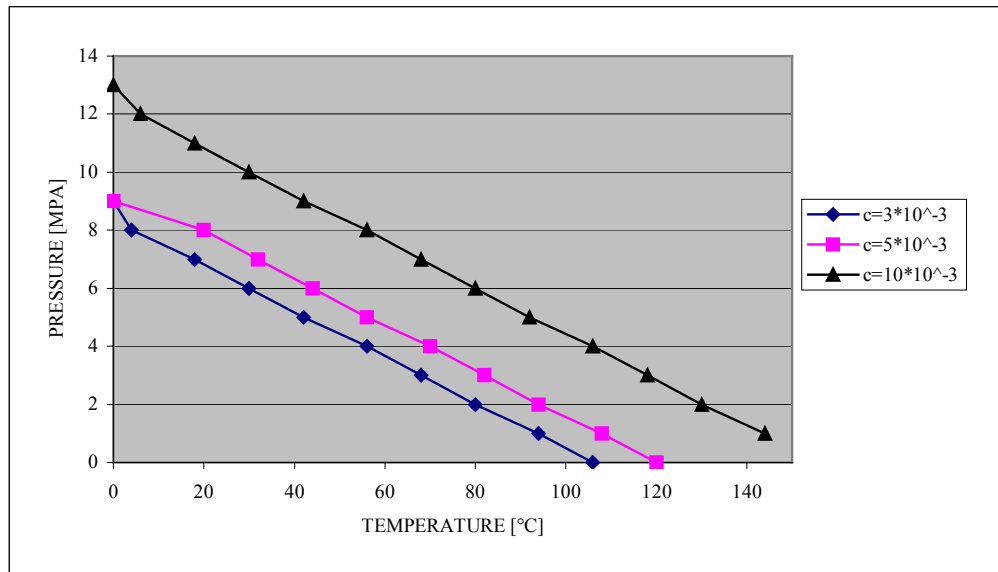


Figure 3.5. Fail pressure of a vessel with [45°/-45°] for linear temperature distribution

As it can be followed from Figure 3.1 and 3.5, the results for parabolic and linear temperature distribution are almost similar.

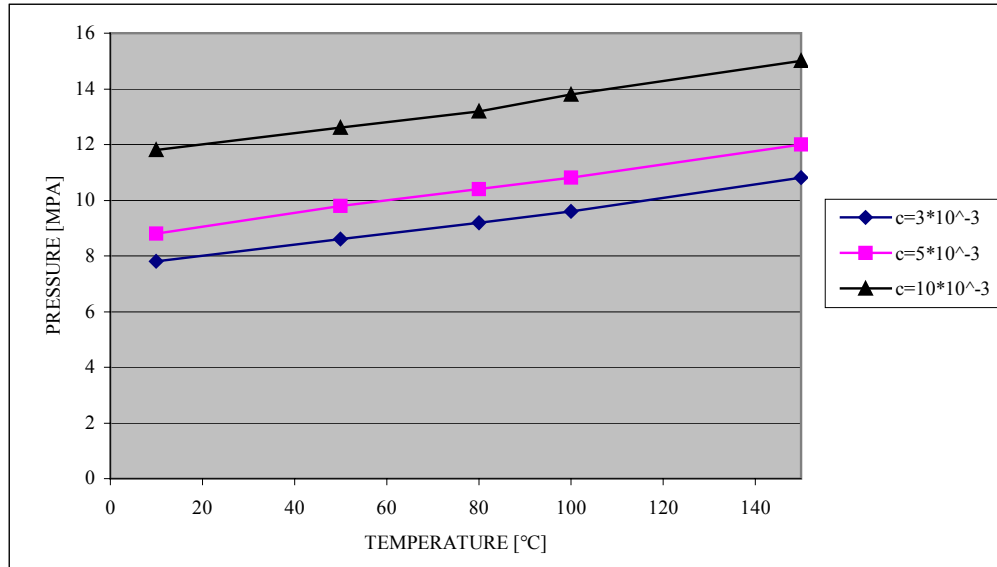


Figure 3.6. Fail pressure of a vessel with  $[45^\circ/-45^\circ]$  for constant temperature distribution

It is seen from Figure 3.6 that, the failure pressure for all the moisture concentration increases when temperature is increased. The tube is subjected to compressive axial stresses, since its axial hygrothermal expansion is prevented by rigid planes at the ends. As a result of this, the tube has a large axial compressive stress at the high temperatures. This compressive stress component increases the failure pressure. This negative effect of temperature can be seen for constant temperature distribution, since both inside and outside of the tube are heated, hence  $\Delta T$  results greater compressive axial stress compared with parabolic temperature distribution, since temperature difference for parabolic temperature distribution is highest at the inside of the tube which is equal to  $T_0$ , where it is  $T_0$  for the whole structure with constant temperature distribution.

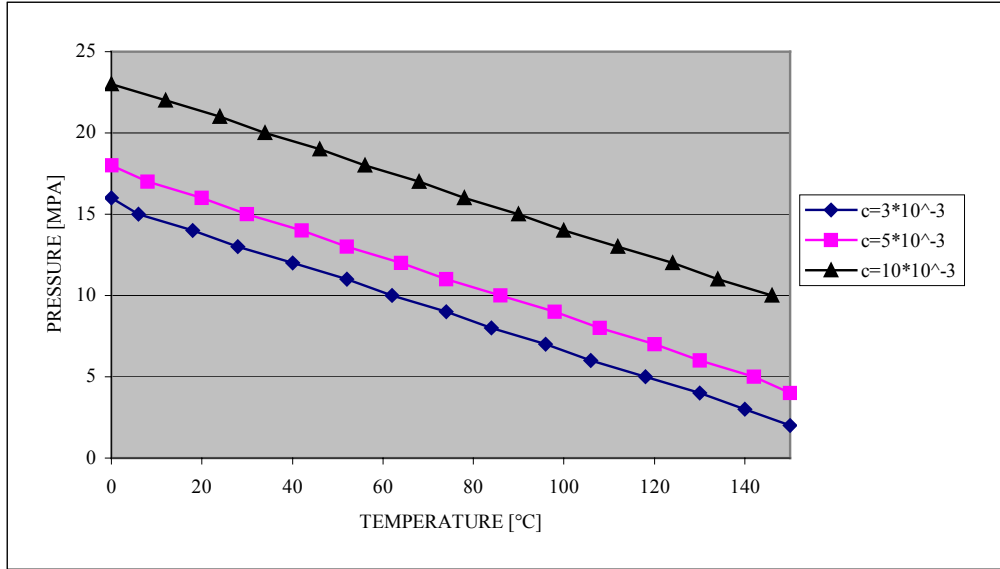


Figure 3.7. Fail pressure of a vessel with [60°/-60°] for parabolic temperature distribution

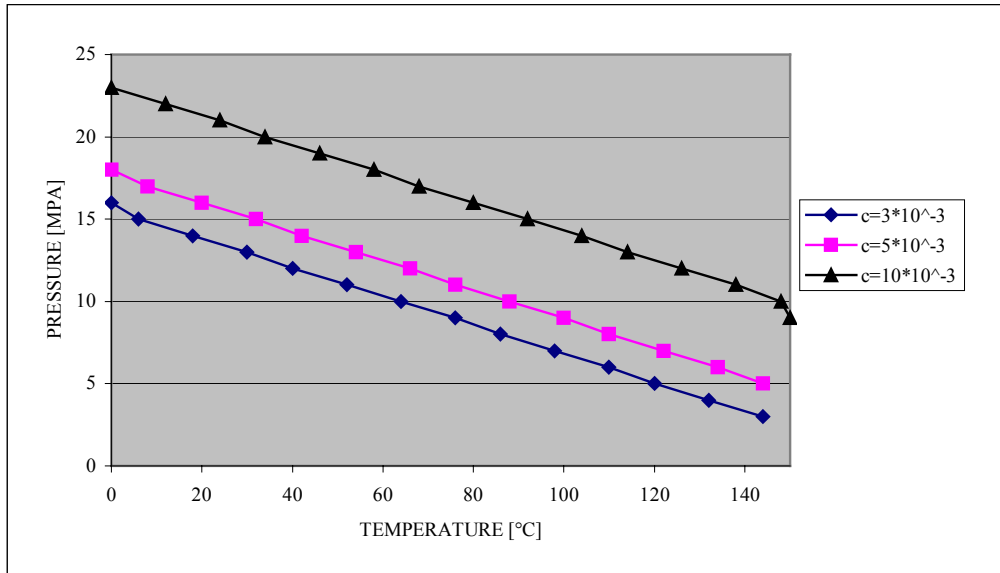


Figure 3.8. Fail pressure of a vessel with [60°/-60°] for linear temperature distribution

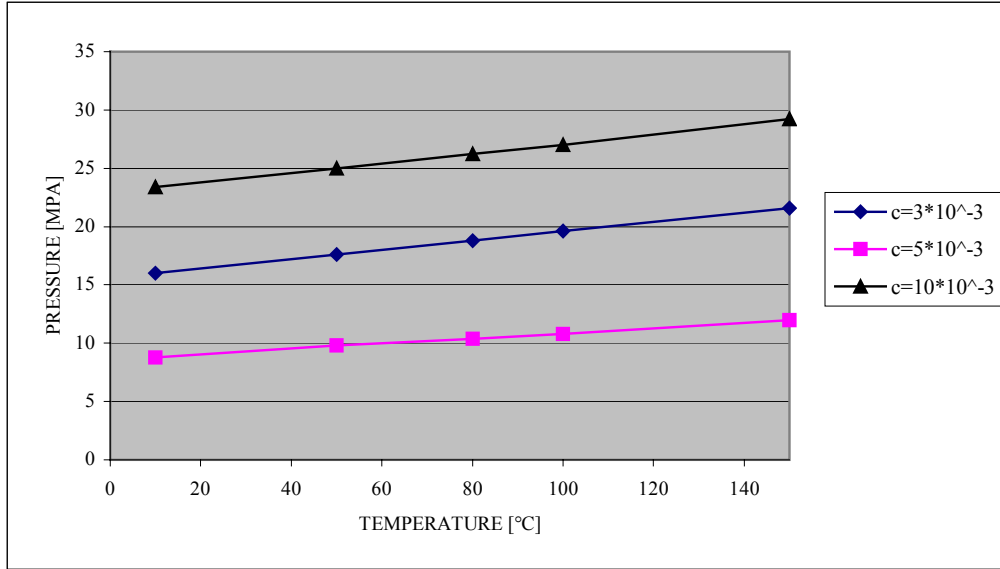


Figure 3.9. Fail pressure of a vessel with [60°/-60°] for constant temperature distribution

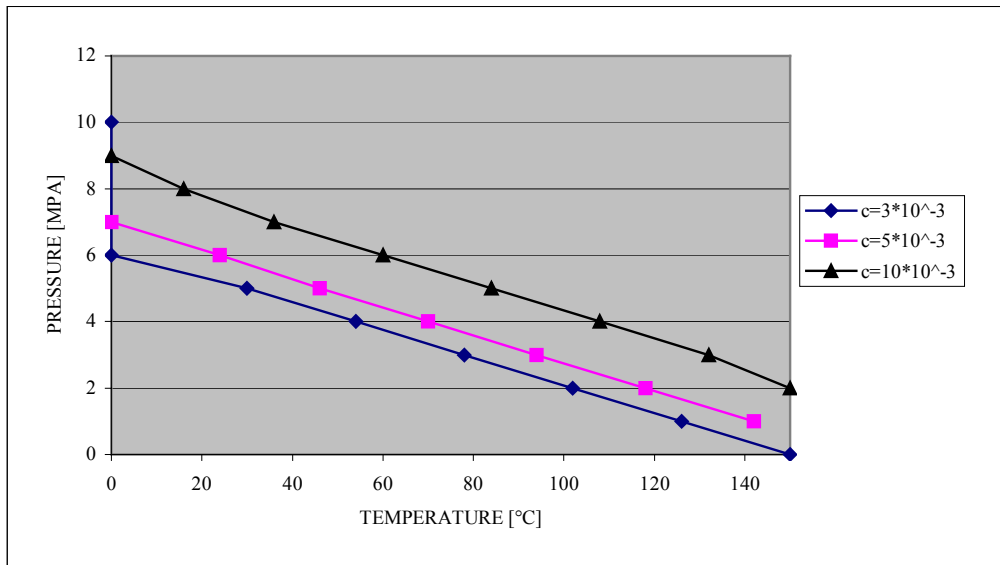


Figure 3.10. Fail pressure of a vessel with [30°/-30°] for parabolic temperature distribution

As it can be seen from the results, the tube, which is layered with the fibers  $\theta = 30^\circ$ , fails mostly at the lower internal pressure comparing with the angle  $45^\circ$  and  $60^\circ$ , since the stress components on the matrix plane, which is weak, can be written as:

$$\sigma_m = \sigma_{zz} \cdot \cos^2(-60) + \sigma_{\theta\theta} \cdot \sin^2(-60) \text{ where } \cos(-60)=0.5 \text{ and } \sin(-60)=0.866$$

$\sigma_{\theta\theta}$  has usually greater value than  $\sigma_{zz}$ . On this plane, the projection of  $\sigma_{\theta\theta}$ , which is calculated as  $(0.866)^2 * \sigma_{\theta\theta}$ , causes failure.

For the tube with the fibers layered  $60^\circ$ , the stress distribution on the weak matrix plane can be calculated as below

$$\sigma_m = \sigma_{zz} \cdot \cos^2(-30) + \sigma_{\theta\theta} \cdot \sin^2(-30) \text{ where } \cos(-30)=0.866 \text{ and } \sin(-30)=0.5$$

For same internal pressure, the material with the fiber  $60^\circ$  resists on the higher pressure where the tube with the fibers layered  $30^\circ$  fails.

For  $\alpha = 45$ ,  $\sigma_m$  is calculated as

$$\sigma_m = \sigma_{zz} \cdot \cos^2(-45) + \sigma_{\theta\theta} \cdot \sin^2(-45) \text{ where } \cos(-45)=0.7077 \text{ and } \sin(-45)=0.707$$

The results of the tube with the fibers layered  $45^\circ$  are between  $30^\circ$  and  $60^\circ$ , since the projection constants are between them.

As a result, it can be concluded that under the same hygrothermal effect, the material with the fibers layered  $30^\circ$  fails mostly at the lower internal pressure than  $60^\circ$  and  $45^\circ$  or it can be also said that at the same internal pressure, a tube with the fibers layered  $30^\circ$  fails at lower temperature than  $60^\circ$  and  $45^\circ$ .

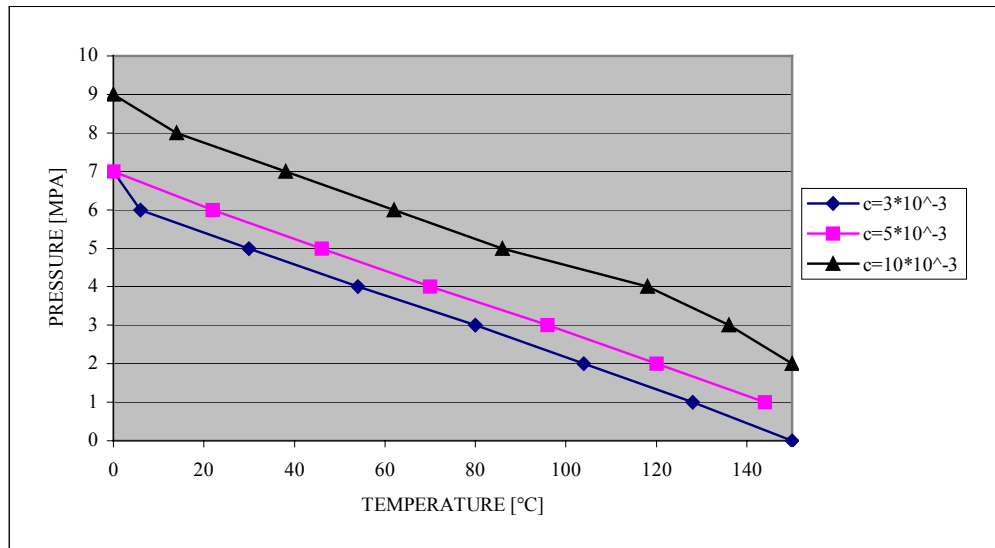


Figure 3.11. Fail pressure of a vessel with  $[30^\circ/-30^\circ]$  for linear temperature distribution

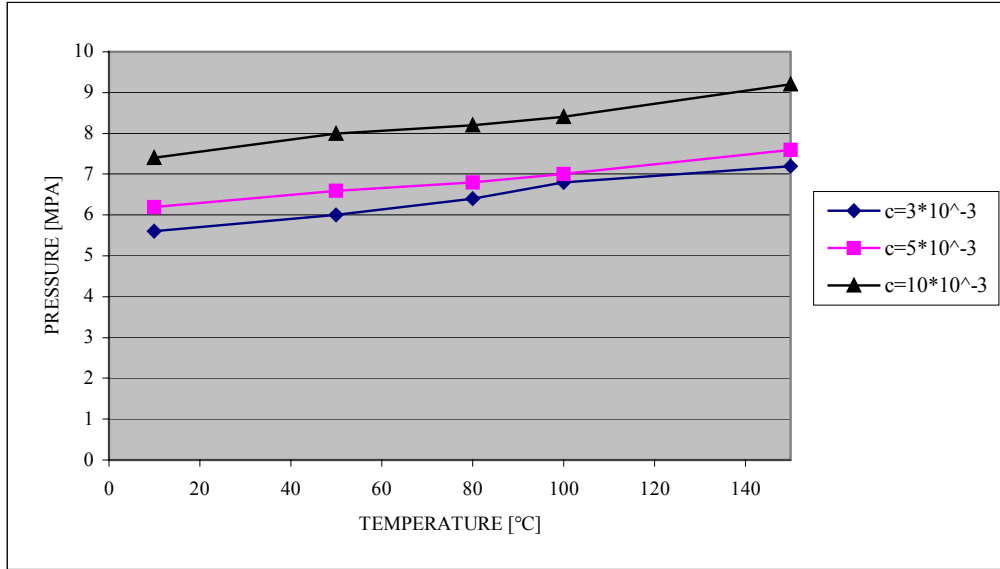


Figure 3.12. Fail pressure of a vessel with for [30°/-30°] for constant temperature distribution

### 3.2 Pressure Vessel

The results of the pressure vessel case are summarized in the following:

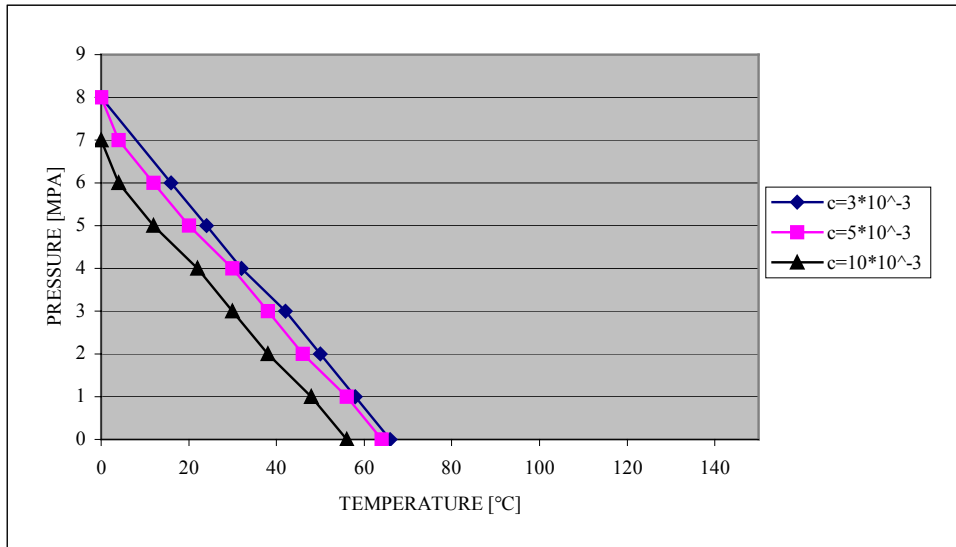


Figure 3.13. Fail pressure of a pressure vessel with [45°/-45°] for parabolic temperature distribution

The resultant stress of the axial stresses in a pressure vessel gives  $\pi a^2 P$ , hence for the absence of internal pressure, the resultant stress gives 0. This can be followed in

Table 3.7-9, where the stress distributions of the pressure vessel with 45° layered fibers and parabolic temperature distribution for different moisture concentrations  $c=3*10^{-3}$ ,  $10*10^{-3}$ ,  $20*10^{-3}$  with the internal pressure value of 0MPa and temperature of 0° C are tabulated.

With increasing moisture concentration, the Hoffman index is also increasing.

$$c=3*10^{-3} \Rightarrow \sigma_m = 2.25 * \cos^2(-45) + 3.04 * \sin^2(-45) = 2.645MPa$$

$$c=10*10^{-3} \Rightarrow \sigma_m = 7.44 * \cos^2(-45) + 10.13 * \sin^2(-45) = 4.285MPa$$

$$c=20*10^{-3} \Rightarrow \sigma_m = 14.85 * \cos^2(-45) + 20.26 * \sin^2(-45) = 17.11MPa$$

Table 3.7. The stress distribution for  $c=3*10^{-3}$

Surface	D	$\sigma_{rr}$	$\sigma_{\theta\theta}$	$\sigma_{zz}$
1	30	0,00	-3,30	-2,49
2	31	-0,08	-1,56	-1,20
3	32	-0,10	0,07	0,02
4	33	-0,07	1,59	1,16
5	34	0	3,04	2,25

The Hoffman index is calculated as  $4.9160*10^{-2}$  for the moisture concentration of  $3*10^{-1}$ .

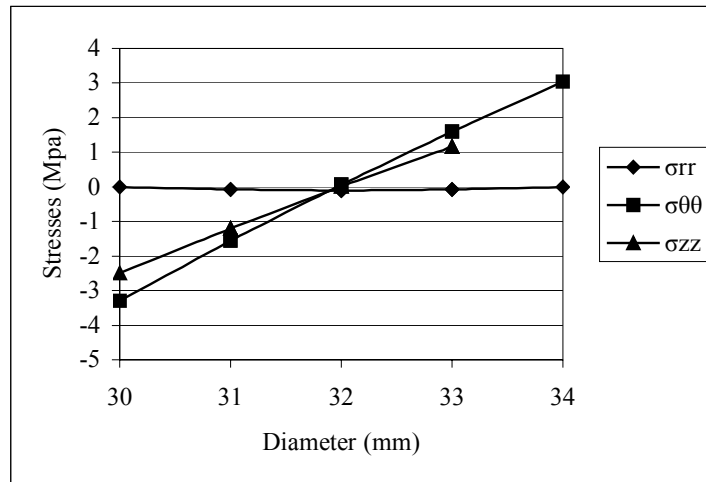


Figure 3.14. The stress distribution for  $c=3*10^{-3}$

Table 3.8. The stress distribution  $c=10 \cdot 10^{-3}$

Surface	D	$\sigma_{rr}$	$\sigma_{\theta\theta}$	$\sigma_{zz}$
1	30	0,00	-11,01	-8,35
2	31	-0,26	-5,20	-4,03
3	32	-0,33	0,22	0,01
4	33	-0,23	5,31	3,82
5	34	0,00	10,13	7,44

The Hoffman index is calculated as  $1.7265 \cdot 10^{-1}$  for the moisture concentration of  $10 \cdot 10^{-1}$

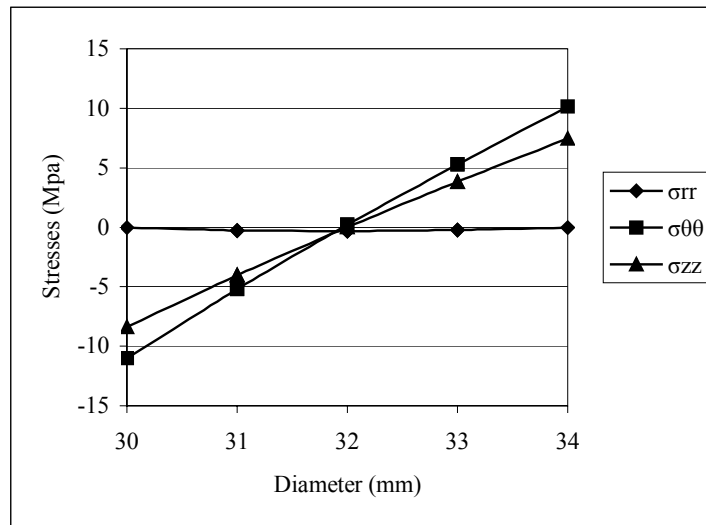


Figure 3.15. The stress distribution for  $c=10 \cdot 10^{-3}$

Table 3.9. The stress distribution for  $c=20 \cdot 10^{-3}$

Surface	D	$\sigma_{rr}$	$\sigma_{\theta\theta}$	$\sigma_{zz}$
1	30	0,00	-22,01	-16,72
2	31	-0,52	-10,40	-8,09
3	32	-0,66	0,44	0,00
4	33	-0,47	10,62	7,62
5	34	0,00	20,26	14,85

The Hoffman index is calculated as  $3.7138 \cdot 10^{-1}$  for the moisture concentration of  $20 \cdot 10^{-1}$ .

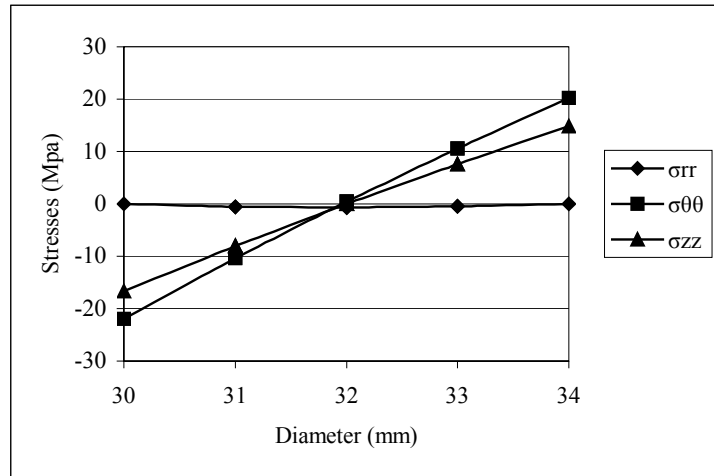


Figure 3.16. The stress distribution for  $c=20 \cdot 10^{-3}$

As moisture concentration increases, the absolute value of the stresses increases also. Axial stress is tensile at the outer surface and compressive at the inner surface of the tube. Because of the tensile stress at the outer surface, the vessel fails at the lower temperature rate with the increasing moisture concentration. In Table 3.10, for different moisture concentrations, the fail temperatures are given where internal pressure is absent.

Table 3.10. Fail temperatures for various moisture concentrations

<b>c</b>	$3 \cdot 10^{-3}$	$5 \cdot 10^{-3}$	$10 \cdot 10^{-3}$	$20 \cdot 10^{-3}$	$30 \cdot 10^{-3}$	$40 \cdot 10^{-3}$	$50 \cdot 10^{-3}$
<b>T<sub>fail</sub></b>	66	64	56	40	26	10	0

Table 3.11. The stress distribution at  $P=1\text{MPa}$ ,  $T=0^\circ\text{C}$

<b>Surface</b>	<b>D</b>	<b>σ<sub>rr</sub></b>	<b>σ<sub>θθ</sub></b>	<b>σ<sub>zz</sub></b>
1	30	-1,00	5,11	1,53
2	31	0,78	6,34	2,46
3	32	0,54	7,52	3,37
4	33	-0,28	8,67	4,25
5	34	0,00	9,80	5,12

The Hoffman index is calculated as  $H=1.4488 \cdot 10^{-1}$ .

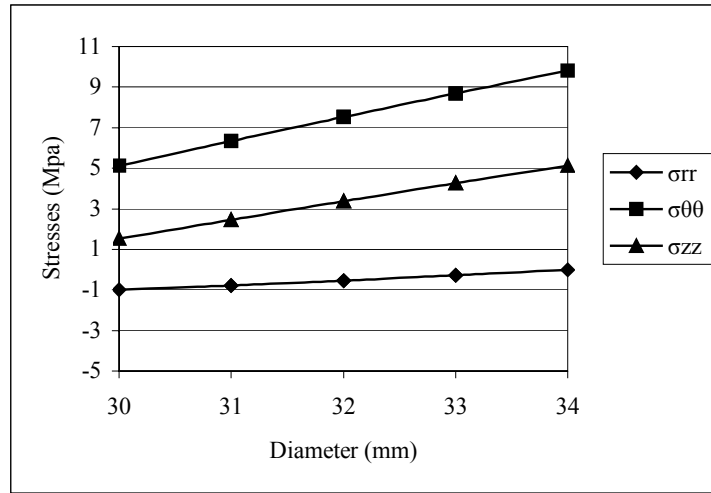


Figure 3.17. The stress distribution at P=1MPa, T=0°C

Table 3.12. The stress distribution at P=7MPa T=0°C

Surface	D	$\sigma_{rr}$	$\sigma_{\theta\theta}$	$\sigma_{zz}$
1	30	-7,00	55,52	26,47
2	31	-5,01	53,68	25,26
3	32	-3,20	52,26	24,34
4	33	-1,54	51,20	23,69
5	34	0,00	50,44	23,24

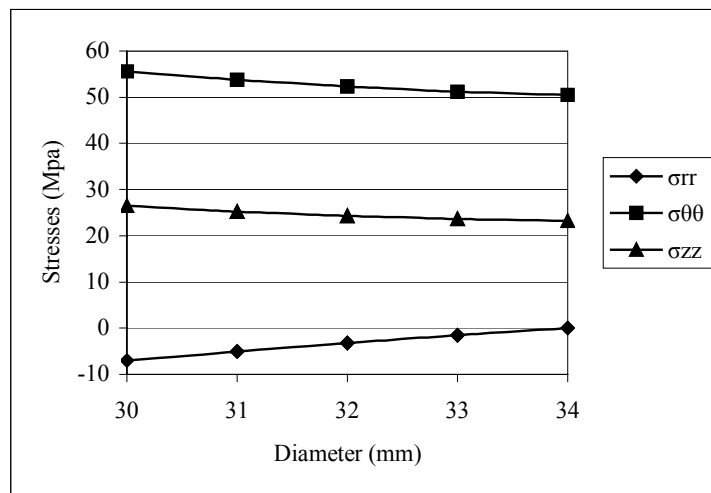


Figure 3.18. The stress distribution at P=7MPa, T=0°C

If the stresses tabulated in Table 3.12 are compared with the stress values given in Table 3.11 where internal pressure is 1MPa and other conditions are same, it can be easily concluded that the stress values are bigger at the internal pressure value of 7MPa. The Hoffman index is calculated as 1.0113, hence the tube fails at 0°C.

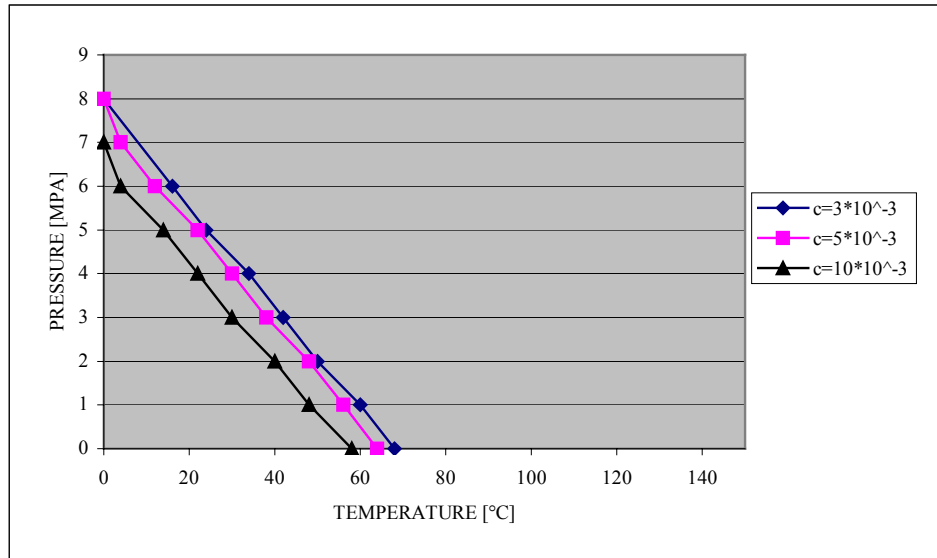


Figure 3.19. Fail pressure of a pressure vessel with [45°/-45°] for linear temperature distribution

As it can be seen from Figure 3.19, the results are similar compared with parabolic temperature distribution.

Table 3.13. Fail pressure of a pressure vessel with [45°/-45°] for constant temperature distribution

$c=3*10^{-3}$		$c=5*10^{-3}$		$c=10*10^{-3}$	
T	P	T	P	T	P
10	7.00	10	7.00	10	7.40
50	7.00	50	7.20	50	7.40
80	7.00	80	7.20	80	7.20
100	7.20	100	7.20	100	7.20
150	7.20	150	7.40	150	7.20

It is seen from Table 3.13, the failure pressure does not change much at the high temperatures for pressure vessels. The ends of the vessels are free for the hygrothermal expansions. As a result of this, the axial stress component is affected

very small at the high temperatures. If the vessel is manufactured by 0 and 90 oriented plies ,the axial stress has high stress values, since different oriented plies apply internal forces each other.

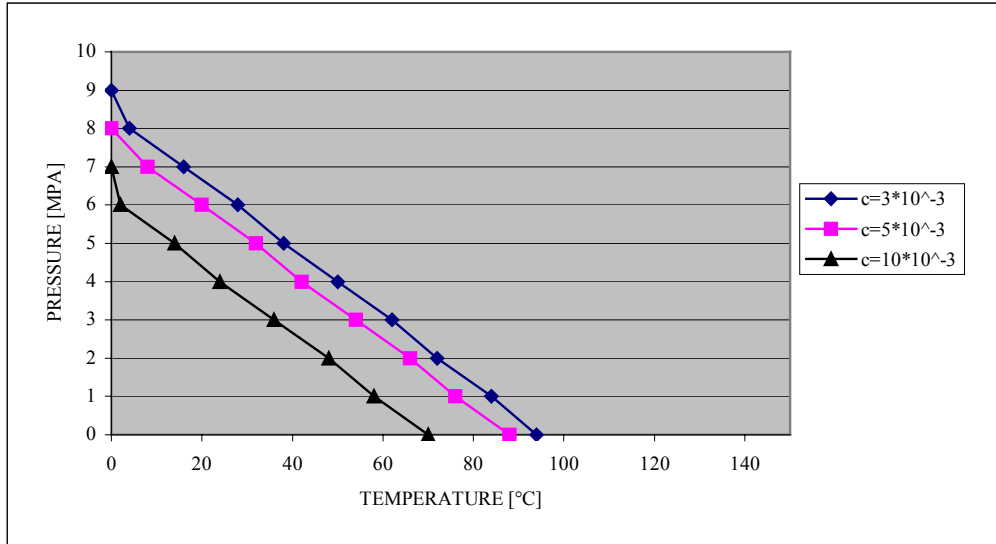


Figure 3.20. Fail pressure of pressure vessel with [60°/-60°] for parabolic temperature distribution

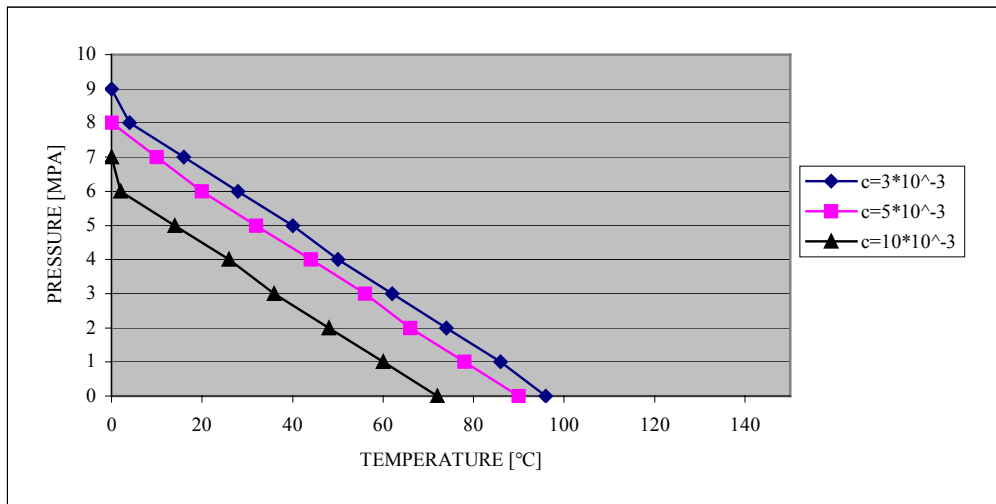


Figure 3.21. Fail pressure of a pressure vessel with [60°/-60°] for linear temperature distribution

Table 3.14. Fail pressure of a pressure vessel with  $[60^\circ/-60^\circ]$  for constant temperature distribution

$c=3*10^{-3}$		$c=5*10^{-3}$		$c=10*10^{-3}$	
T	P	T	P	T	P
10	8.40	10	7.80	10	6.40
50	8.00	50	7.40	50	6.00
80	7.80	80	7.20	80	5.60
100	7.60	100	7.00	100	5.40
150	7.00	150	6.40	150	5.00

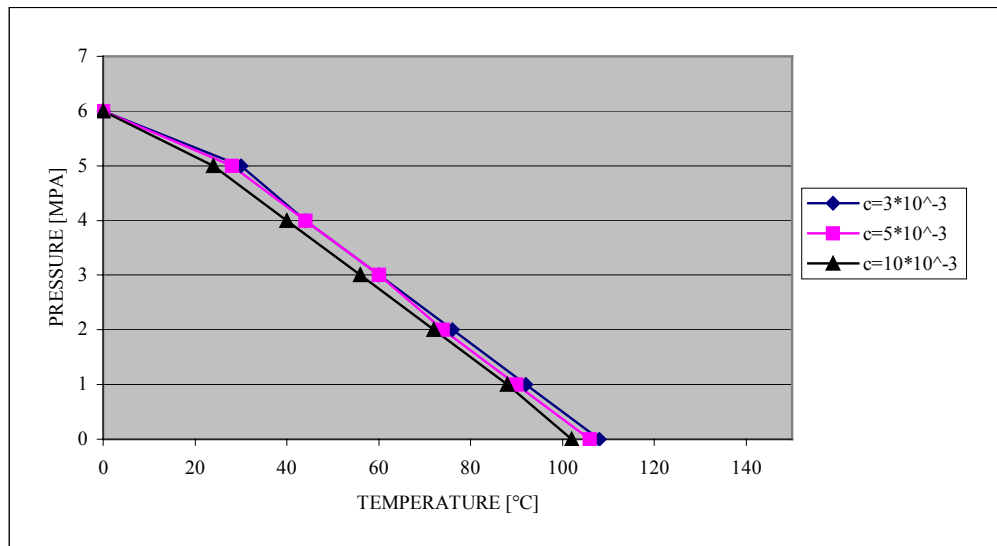


Figure 3.22. Fail pressure of a pressure vessel with  $[30^\circ/-30^\circ]$  for parabolic temperature distribution

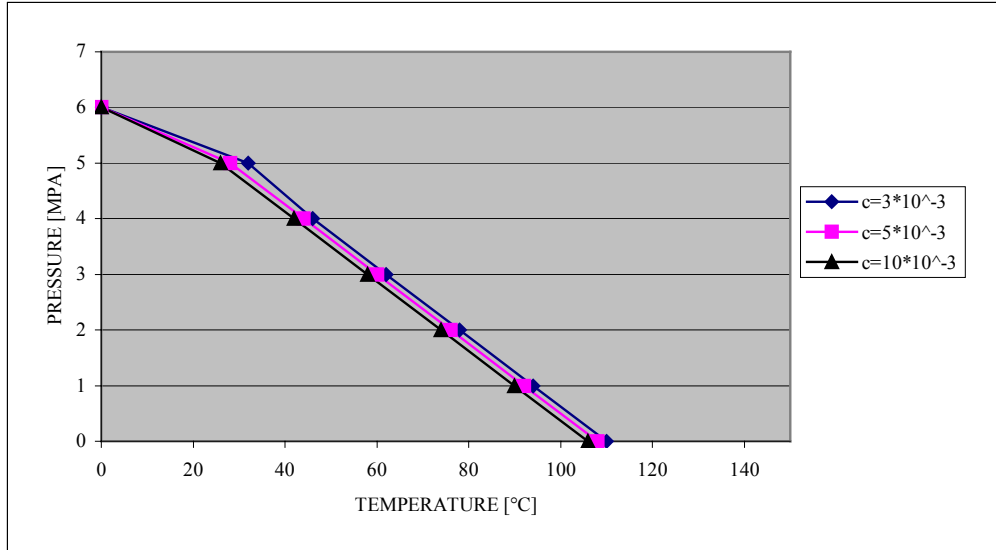


Figure 3.23. Fail pressure of a pressure vessel with [30°/-30°] for linear temperature distribution

Table 3.15. Fail pressure of a pressure vessel with [30°/-30°] for constant temperature distribution

c=3*10 <sup>-3</sup>		c=5*10 <sup>-3</sup>		c=10*10 <sup>-3</sup>	
T	P	T	P	T	P
10	4.80	10	5.60	10	5.60
50	5.60	50	5.60	50	5.60
80	5.60	80	5.60	80	5.60
100	5.60	100	5.60	100	5.60
150	5.60	150	5.60	150	5.60

### 3.3. Free-End Case

The results of the vessel with free-end case are summarized in the following graphs:

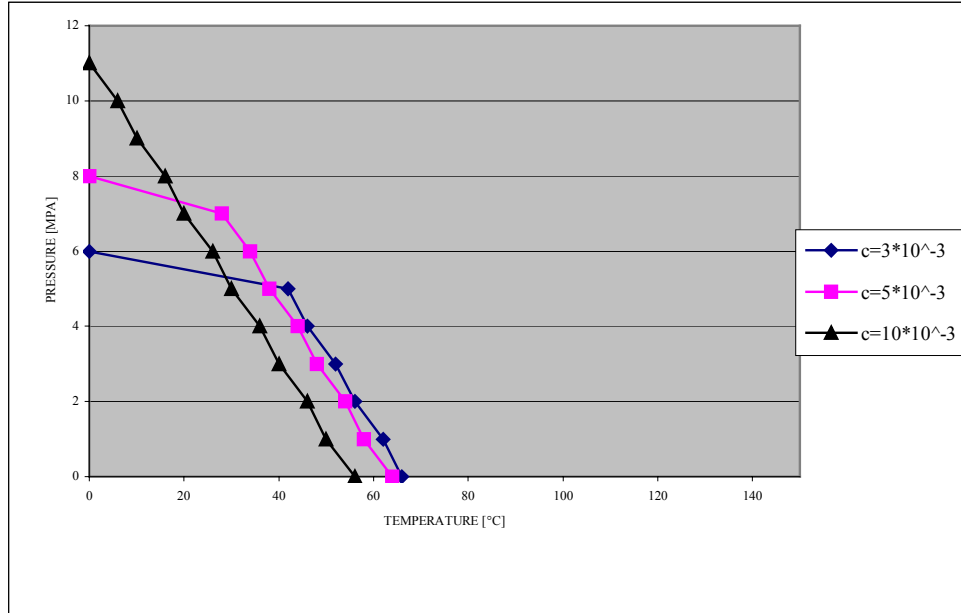


Figure 3.24. Fail pressure of a vessel with [45°/-45°] for parabolic temperature distribution

In order to investigate the effect of the moisture concentration on the tube with free ends, the stress distributions for three different moisture concentrations of  $3 \cdot 10^{-3}$ ,  $5 \cdot 10^{-3}$  and  $10 \cdot 10^{-3}$  are tabulated in Table 3.16-18.

Table 3.16. The stress distribution for  $c=3 \cdot 10^{-3}$

Surface	D	$\sigma_{rr}$	$\sigma_{\theta\theta}$	$\sigma_{zz}$
1	30	0,00	-3,30	-2,49
2	31	-0,08	-1,56	-1,20
3	32	0,10	0,07	0,02
4	33	-0,07	1,59	1,16
5	34	0,00	3,04	2,25

The Hoffman index is calculated as  $4.9160 \cdot 10^{-2}$ .

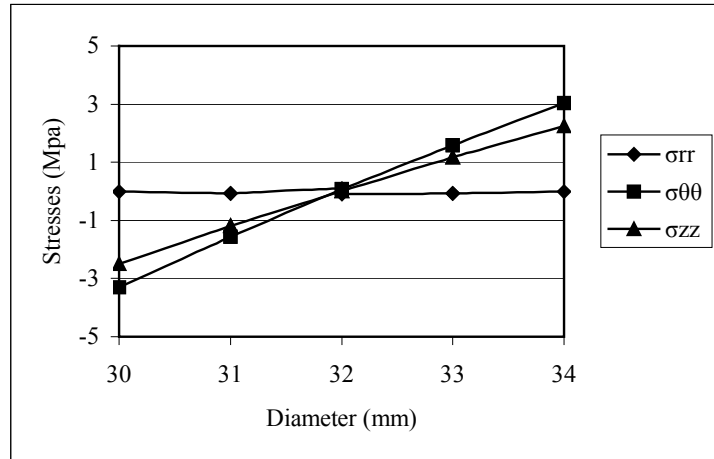


Figure 3.25. The stress distribution for the moisture concentration of  $3 \cdot 10^{-3}$

Table 3.17. The stress distribution for  $c=10 \cdot 10^{-3}$

Surface	D	$\sigma_{rr}$	$\sigma_{\theta\theta}$	$\sigma_{zz}$
1	30	0,00	-11,01	-8,35
2	31	-0,26	-5,20	-4,03
3	32	-0,33	0,22	0,01
4	33	-0,23	5,31	3,82
5	34	0,00	10,13	7,44

where the Hoffman index is calculated as  $1.7265 \cdot 10^{-1}$

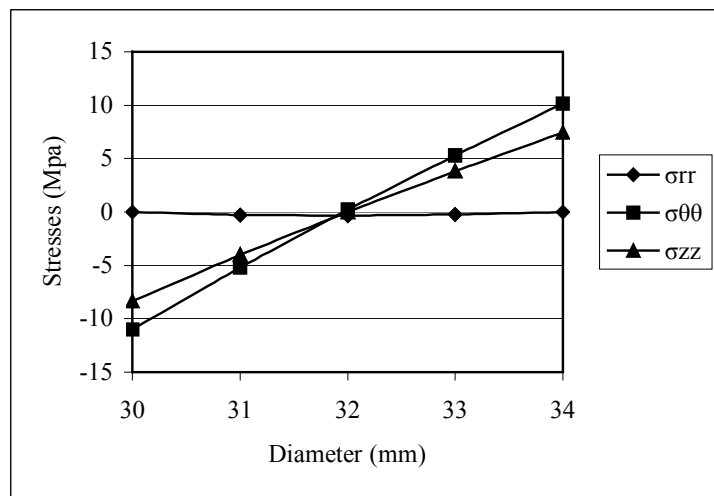


Figure 3.26. The stress distribution for the moisture concentration of  $10 \cdot 10^{-3}$

Table 3.18. The stress distribution for  $c=20*10^{-3}$

Surface	D	$\sigma_{rr}$	$\sigma_{\theta\theta}$	$\sigma_{zz}$
1	30	0,00	-22,01	-16,72
2	31	-0,52	-10,40	-8,09
3	32	-0,66	0,44	0,00
4	33	-0,47	10,62	7,62
5	34	0,00	20,26	14,85

where the Hoffman index is calculated as  $3.7138*10^{-1}$

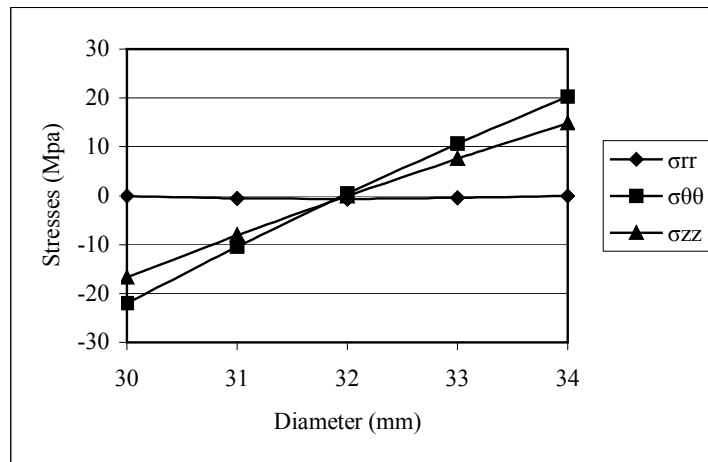


Figure 3.27. The stress distribution for the moisture concentration of  $20*10^{-3}$

As it can be seen from Tables 3.16-18, with increasing moisture concentration the absolute value of axial, tangential and radial stresses and as result of this, the Hoffman index increase also. In Table 3.19, the fail temperatures for different moisture concentration values are presented.

Table 3.19. Fail temperatures of a tube for various moisture concentrations

c	$3*10^{-3}$	$5*10^{-3}$	$10*10^{-3}$	$20*10^{-3}$	$30*10^{-3}$	$40*10^{-3}$	$50*10^{-3}$
$T_{fail}$	66	64	56	40	26	10	0

In Table 3.20, the stress distributions for the moisture concentration of  $3 \cdot 10^{-3}$  with the temperature value of  $66^\circ\text{C}$  and internal pressure of  $0\text{MPa}$  are presented as

Table 3.20. The stress distribution at  $T=66^\circ\text{C}$

Surface	D	$\sigma_{rr}$	$\sigma_{\theta\theta}$	$\sigma_{zz}$
1	30	0,00	-41,61	-41,13
2	31	-1,00	-20,53	-20,99
3	32	-1,29	0,15	-0,95
4	33	-0,93	20,61	19,12
5	34	0,00	40,99	39,33

The Hoffman index is calculated as  $H=1.0049$ .

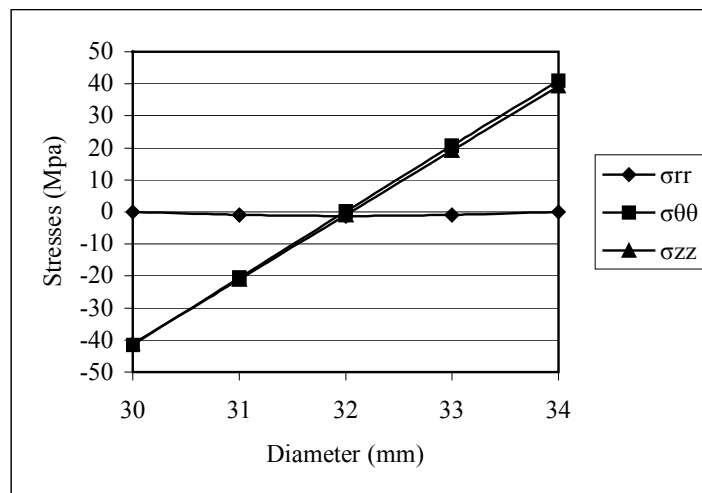


Figure 3.28. The stress distribution at  $P=0\text{MPa}$ ,  $T=66^\circ\text{C}$

In Table 3.16, all the conditions are identical with the conditions presented in Table 3.21 except the temperature. In Table 3.17, temperature is  $0^\circ\text{C}$ , whereas in Table 3.21,  $66^\circ\text{C}$ . It can be easily seen from these tables that the absolute value of the stresses increases at  $T=66^\circ\text{C}$  compared with  $T=0^\circ\text{C}$ .  $T=66^\circ\text{C}$  is the fail temperature at the given conditions, as the Hoffman index is calculated greater than 1.

In order to see the pressure effect, the results are tabulated for two different pressure rates, where other conditions have been kept same. In Tables 3.21 and 3.22, the stress distributions of a tube with free ends for parabolic temperature distribution

and the moisture concentration of  $5 \cdot 10^{-3}$  with the internal pressure values of 1MPa and 6MPa are presented.

Table 3.21. The stress distribution at P=1MPa, T=0°C

Surface	D	$\sigma_{rr}$	$\sigma_{\theta\theta}$	$\sigma_{zz}$
1	30	-1,00	3,24	-3,27
2	31	-0,83	5,45	-1,61
3	32	-0,60	7,56	-0,01
4	33	-0,32	9,58	1,52
5	34	0,00	11,52	2,99

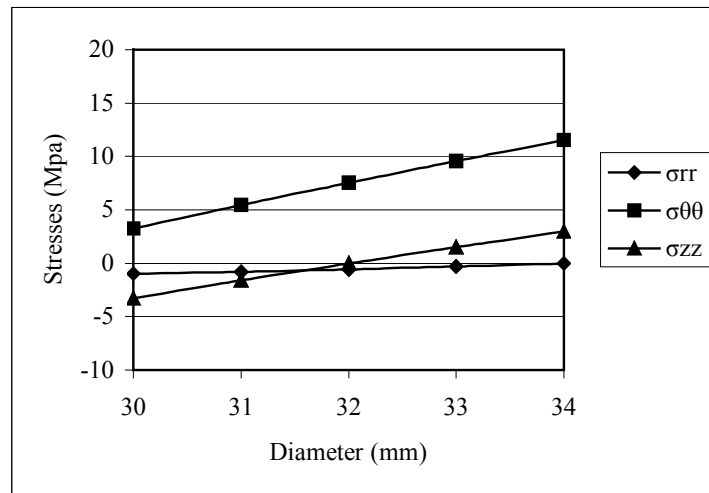


Figure 3.29. The stress distribution at P=1MPa, T=0°C

Table 3.22. The stress distribution at P=6MPa, T=0°C

Surface	D	$\sigma_{rr}$	$\sigma_{\theta\theta}$	$\sigma_{zz}$
1	30	-6,00	46,96	1,22
2	31	-4,31	45,72	0,43
3	32	-2,76	44,81	-0,13
4	33	-1,33	44,19	-0,47
5	34	0,00	43,81	-0,64

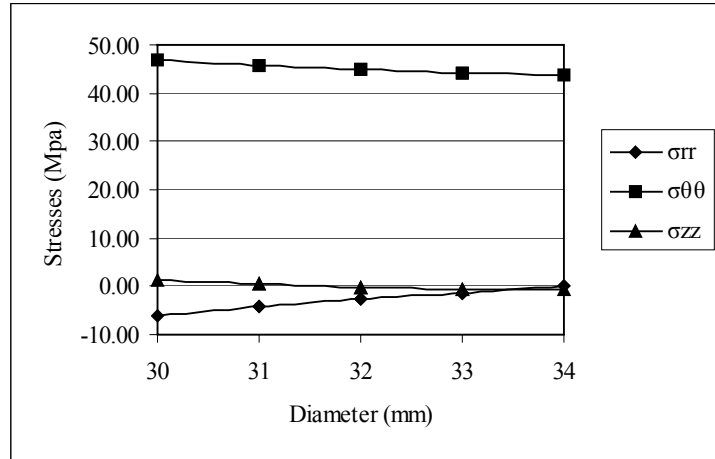


Figure 3.30. The stress distribution at P=6MPa, T=0°C

As it can be seen from these graphs, tangential stresses and radial stresses increase with increasing pressure.

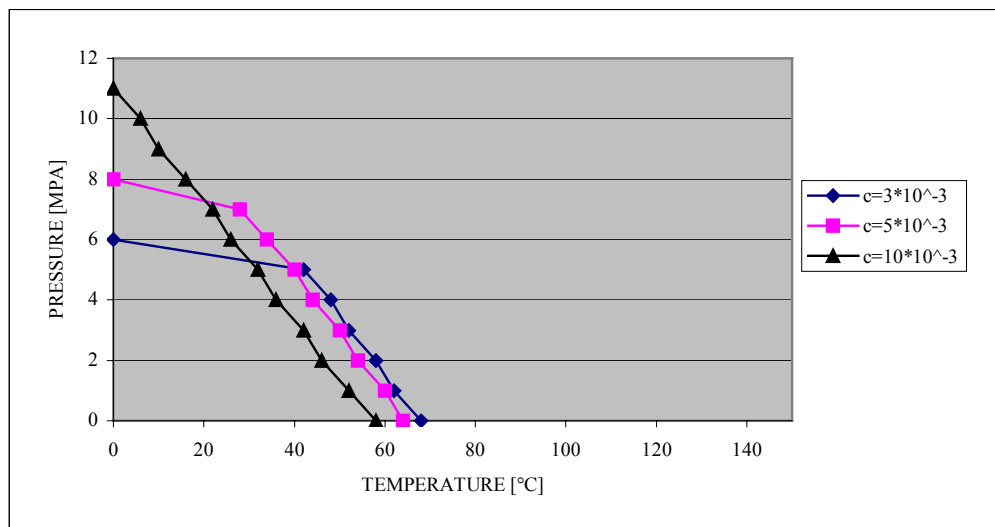


Figure 3.31. Fail pressure of a vessel with [45°/-45°] for linear temperature distribution

Table 3.23. Fail pressure of vessel with [45°/-45°] for constant temperature distribution

$c=3*10^{-3}$		$c=5*10^{-3}$		$c=10*10^{-3}$	
T	P	T	P	T	P
10	7.00	10	7.00	10	7.40
50	7.00	50	7.20	50	7.40
80	7.00	80	7.20	80	7.20
100	7.20	100	7.20	100	7.20
150	7.20	150	7.40	150	7.20

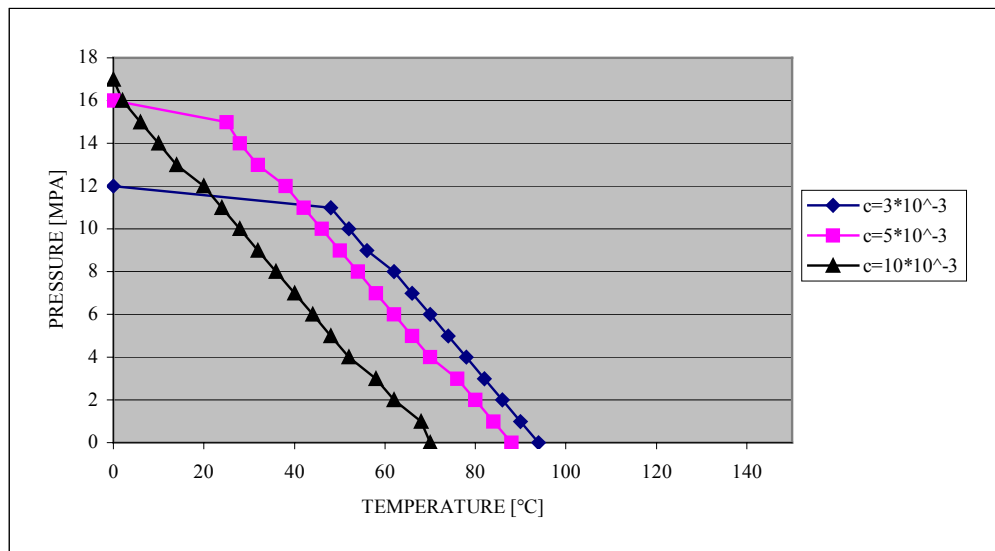


Figure 3.32. Fail pressure of vessel with [60°/-60°] for parabolic temperature distribution

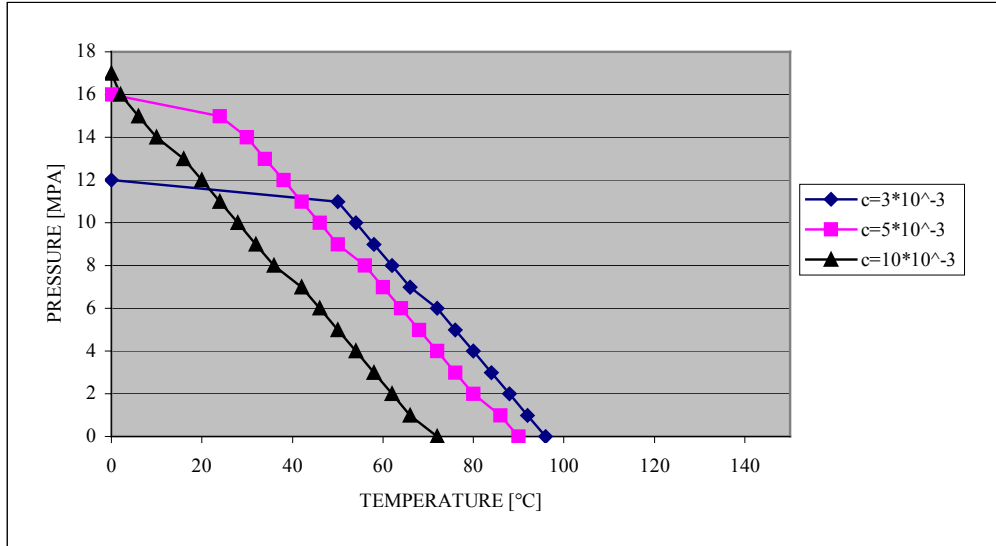


Figure 3.33. Fail pressure of vessel with free ends for [60°/-60°] for linear temperature distribution

Figure 3.24. Fail pressure of vessel with [60°/-60°] for constant temperature distribution

$c=3*10^{-3}$		$c=5*10^{-3}$		$c=10*10^{-3}$	
T	P	T	P	T	P
10	8.40	10	7.80	10	6.40
50	8.00	50	7.40	50	6.00
80	7.80	80	7.20	80	5.60
100	7.60	100	7.00	100	5.40
150	7.00	150	6.40	150	5.00

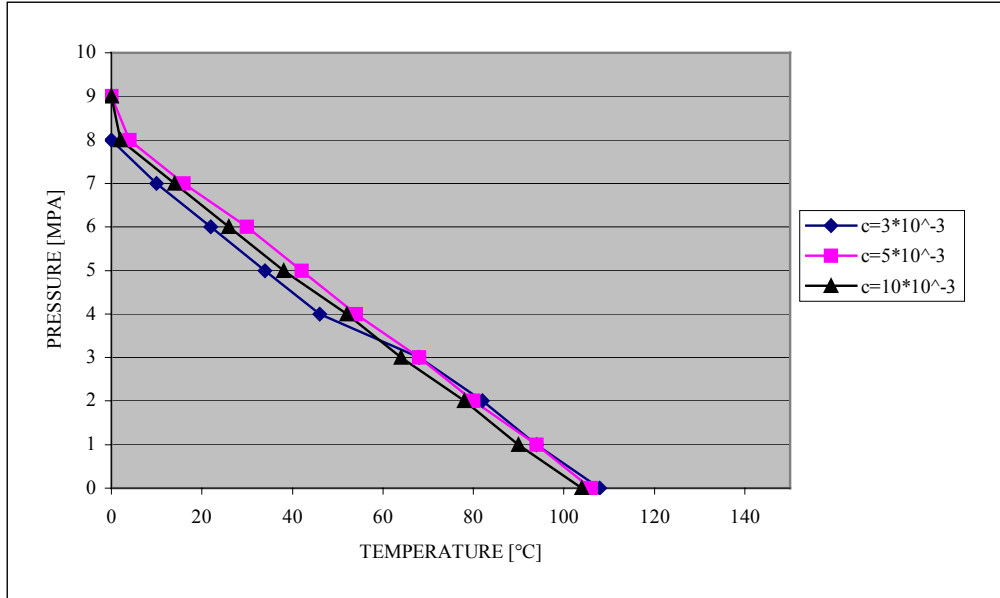


Figure3.34. Fail pressure of vessel with [30°/-30°] for parabolic temperature distribution

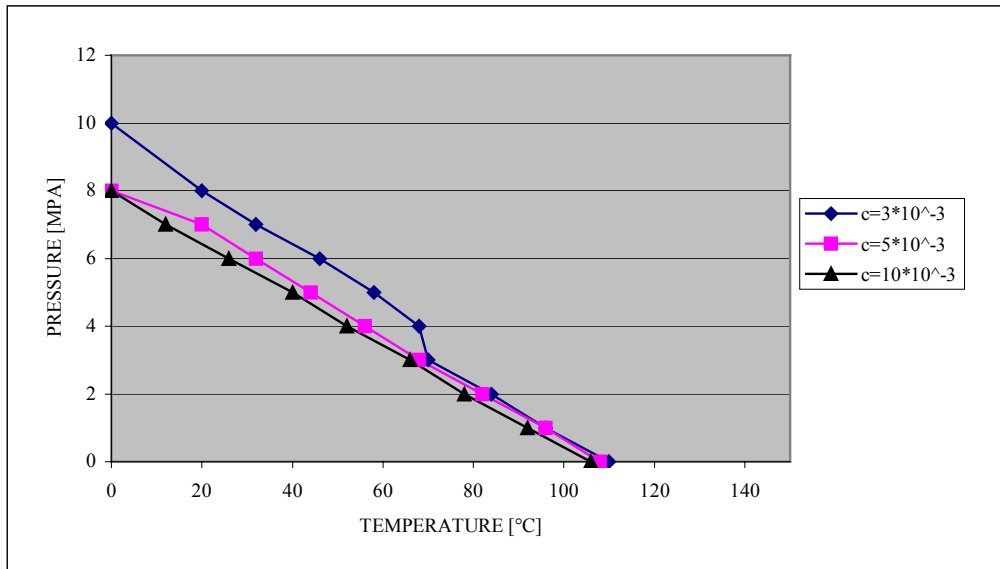


Figure 3.35. Fail pressure of vessel with [30°/-30°] for linear temperature distribution

Figure 3.25. Fail pressure of vessel with [30°/-30°] for constant temperature distribution

$c=3*10^{-3}$		$c=5*10^{-3}$		$c=10*10^{-3}$	
T	P	T	P	T	P
10	4.80	10	5.60	10	5.60
50	5.60	50	5.60	50	5.60
80	5.60	80	5.60	80	5.60
100	5.60	100	5.60	100	5.60
150	5.60	150	5.60	150	5.60

### 3.4. Optimum Winding Angle Determination

Mechanical properties of a composite structure are highly dependent on the winding angle used because of the nature of the fiber-reinforced composite materials. To obtain a mechanical structure satisfying the needs, determination of the optimum winding angle becomes important.

In Figure 3.36, the Hoffman indexes are presented for different winding angles for a vessel with plane strain case, linear temperature distribution and  $c=10*10^{-3}$ . Hoffman indexes are calculated for each winding angle at  $T=20^{\circ}$  C and  $P=4$  MPA are compared each other. Then, the winding angle with minimum Hoffman index is chosen as optimum winding angle since at the same loading conditions, it results minimum effect on the structure.

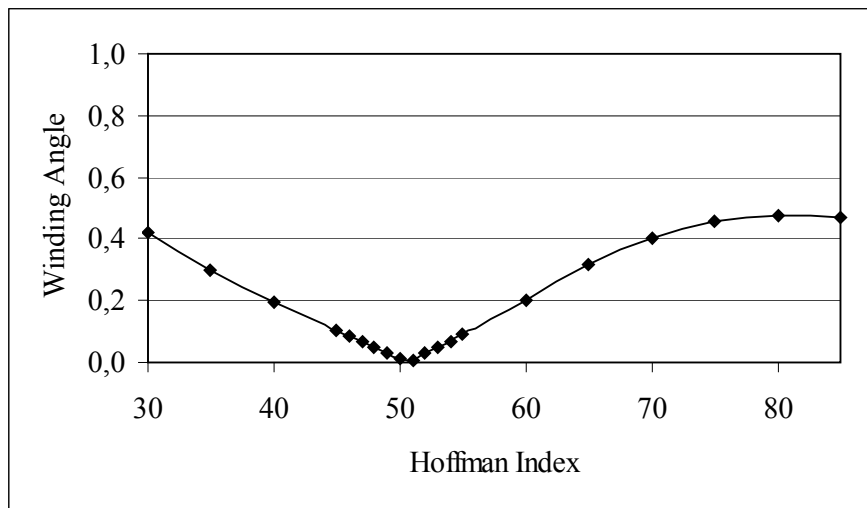


Figure 3.36. Hoffman index comparison for different winding angles

It can be seen from Figure 3.36, that  $\theta = 51^\circ$  is the optimum winding angle for the composite structure with plane strain case.

The stress distribution for  $\theta = 51^\circ$  is presented in Table 3.26.

Table 3.26. The stress distribution at  $\theta = 51^\circ$

<b>Surface</b>	<b>D</b>	<b><math>\sigma_{rr}</math></b>	<b><math>\sigma_{\theta\theta}</math></b>	<b><math>\sigma_{zz}</math></b>
1	30	-5,00	-48,01	-121,98
2	31	-5,66	-3,52	-92,36
3	32	-4,93	38,70	-63,66
4	33	-2,99	79,13	-35,69
5	34	0,00	118,17	-8,26

## CHAPTER 4

### CONCLUSION AND FUTURE RECOMMENDATIONS

In this study, an explicit analytical formulation is developed based on the anisotropic elasticity theory that determines the behavior of fiber reinforced composite vessel under hygrothermal loading. The loading was studied for three cases separately. These are plane strain case in which the tube is prevented to expand and free-end and pressure vessel cases in which the tube is free to expand. Throughout the study, constant, linear and parabolic temperature distributions are investigated and for each distribution, separate equations are developed. The numerical solution enables to investigation of the behavior of the vessel under different hygrothermal and internal pressure conditions. By taking the moisture concentration constant of throughout the body, hygrothermal stresses and displacements are determined.

The tube has been modeled as a set of cylindrically orthotropic layers. Each layer has an angle ply of (+) and (-)  $\alpha$  where  $\alpha$  is the winding angle of any layer. The through thickness elastic constants have been found from the correlations derived from a recent study.

For each layer, two different equations are developed. These are the correlations of radial stress and radial displacements. These relations have been solved using the boundary conditions. Since there are two unknown for each layer and there are  $2*n$  boundary conditions for  $n$  number of layers, the computer program is capable to solve this set of equations.

Throughout the study, two computer programs are developed. The first one is developed for the plane strain case where the other program is both for pressure vessel and free-end cases.

In free-end case, the resultant force along the tube axis is equal to zero, since both ends of the tube are free to expand. On the other hand, for the pressure vessel, the resultant force along the tube is equal to the effect of internal pressure on the caps of the pressure vessel. After finding the stresses, Hoffman failure criteria is applied to investigate the behavior of fiber reinforced composite vessel under the effects of both thermal and moisture. The reason to choose this criteria is that Hoffman criteria gives much more consistent solution when the material has different compressive and tensile strengths.

In this study, it is assumed that the mechanical properties of the material do not change with increasing temperature up to 150° C. After this temperature rate, the material properties will degrade.

From the results, it can be concluded that the results for linear and parabolic temperature distributions give almost the similar results. On the other hand, constant temperature distribution has a different characteristic than the others. For parabolic temperature distribution, with increasing temperature rate, failure pressure decreases, whereas the failure pressure for constant temperature distribution increases for plane strain case. On the other hand, the failure pressure does not change much at the high temperatures for pressure vessels and free ends with constant temperature distribution.

It is found also that the tube, which is layered with the fibers 30°, fails mostly at the lower internal pressure comparing with the angle 45° and 60°, since the stress components on the matrix plane are greater for 30°.

It is concluded from the results that for plane strain case and small moisture concentration values, moisture effect may sometimes act reverse and the tube may fail at higher temperature.

The method developed in this study can be applied to all long composite cylinders, pressure vessels and tanks.

As a future work, the vessel under axisymmetric and non-axisymmetric loading with the internal pressure and hygrothermal effects can be investigated. The vessel under a single force with pressure and hygrothermal effects can be seen in practical applications. Also in these applications, the vessel can have metallic or plastic liners.

## REFERENCES

- [1] TSAI, S. W., *Composite Design*. Think Composites, Ohio, 1987.
- [2] LEKHNITSKII, S., G., *Theory of Elasticity of an Anisotropic Body*, Mir Publishers, Moscow, 1980.
- [3] JONES, R. M., *Mechanics of Composite Materials*, Taylor & Francis, Philadelphia, 1999
- [4] AHÇI, E., *Design of Fiber Reinforced Composite Rocket Motor Case*, Middle East Technical University, 1998.
- [5] ALEÇAKIR, S. *Structural Design and Experimental Analysis of a Filament Wound Composite Tube under Combined Loading*, Middle East Technical University, 1998.
- [6] KATIRCI, N., *Analysis of Fiber Reinforced Composite Pressure Vessel*, Middle East Technical University, 1998.
- [7] XIA, M., TAKAYANAGI, H., KEMMOCHI, K., *Analysis of Multi-layered Filament-wound Composite Pipes under Internal Pressure*, Ministry of International Trade and Industry, 2001
- [8] WIND, P. M., VICKERS, G. W., *Analysis of Filament-wound Cylindrical Shells under Combined Centrifugal, Pressure and Axial Loading*, University of Victoria, 1996
- [9] XIA, M., TAKAYANAGI, H., KEMMOCHI, K., *Analysis of Transverse Loading for Laminated Cylindrical Pipes*, Ministry of International Trade and Industry, 2001
- [10] XIA, M., TAKAYANAGI, H., KEMMOCHI, K., *Analysis of Filament-wound Fiber-reinforced Sandwich Pipe under Combined Internal and Termomechanical Loading*, Ministry of International Trade and Industry, 2001

- [11] TARN, J., WANG, Y., *Laminated Composite Tubes under Extension, Torsion, Bending, Shearing and Pressurizing: a State Space Approach*, National Cheng Kung University, 2000
- [12] LIANG, C., CHEN, H., WANG, C., *Optimum design of Dome Contour for Filament-wound Composite Pressure Vessels Based on a Shape Factor*, Da-Yeh University, 2002
- [13] XIA, M., TAKAYANAGI, H., KEMMOCHI, K., *Bending Behavior of Fiber -Reinforced Sandwich Pipes*, Smart Structure Research Center, Japan, 2002
- [14] VINSON, J. R., CHOU, T. W., *Composite Materials and Their Use in Structures*, Applied Science Publishers Ltd ,1975.
- [15] GIBSON, R.F., *Principles of Composite Material Mechanics*, Mc-Graw-Hill, Inc., 1994
- [16] WEETON, J. W., PETERS, D. M., THOMAS, K. L., *Engineers' Guide to Composite Materials*, American Society for Metals, 1986